ISSN 2718-222X (Online)
ISSN 1334-1219 (Print)
Engineering Power
BULLETIN OF THE CROATIAN ACADEMY OF ENGINEERING Vol. 16(2) 2021

EDITOR-IN-CHIEF'S WORD

Dear readers,

The guest editor of this issue is a member of our Academy from the Department of Mechanical Engineering and Naval Architecture, Prof. Lidija Ćurković, Ph.D, full professor at the Faculty of Mechanical Engineering and Naval Architecture, University of Zagreb.

The research of the author and her collaborators in the field of monolithic and composite ceramics has led to a number of scientific papers, some of which are very interestingly presented in this issue of our publication. I believe that you will read the presented papers with interest.

Editor
Vladimir Andročec, President of the Croatian Academy of Engineering

EDITOR'S WORD

Dear readers,

It is our pleasure to present in this edition of HATZ bulletin Engineering Power prominent scientific research in the domain of production of advanced ceramics carried out at the Faculty of Mechanical Engineering and Naval Architecture, University of Zagreb.

The Guest-Editor of this issue is Lidija Ćurković, Associate Member of the Academy and Professor at the Faculty of Mechanical Engineering and Naval Architecture, University of Zagreb, who presents part of the research activities of the Faculty's Laboratory for Engineering Ceramics.

Since the production and application of new advanced materials is one of the most important fields of modern science and technology, I am sure that you will enjoy reading the presented contributions.

Editor
Zdravko Terze, Vice-President of the Croatian Academy of Engineering

FOREWORD

The production of advanced ceramics as inorganic non-metallic materials is an important and one of the most economically potential branches in the developed countries, which is why it has received a lot of attention in many industrial fields.

The formation of the crucially important microstructure and thereby the desired properties (mechanical, tribological, corrosion resistance, etc.) of the advanced ceramic product are influenced by the appropriate selection of raw materials and additives, the process of forming the so-called green bodies (i.e., presintered bodies), and the sintering process (conventional and non-conventional). This type of "linked" research, which studies the connection between the structure, the forming process, and the modelling of properties to achieve faster engineering applications, is still relatively rare in Croatian science. It represents a much-needed paradigm shift to bring the Croatian scientists closer to the current international trend of goal-oriented problem solving.

The scientific papers summarized below represent a part of the scientific research in the field of monolithic and composite advanced ceramics done by the members of the Laboratory for Engineering Ceramics at the Faculty of Mechanical Engineering and Naval Architecture, University of Zagreb. The presented studies were carried out within the framework of the project "Monolithic and Composite Advanced Ceramics for Wear and Corrosion Protection" (WECOR, IP-2016-06-6000) funded by the Croatian Science Foundation.

The first paper deals with the investigation of the influence of the combinations of three dispersants on the viscosity of highly concentrated aqueous alumina suspensions. The suspensions were used for slip casting forming, and stable suspension composition was statistically optimized. Slip casting is one of the simplest ceramics forming methods. Other forming methods, besides casting, include pressing and plastic forming. Slip casting can be used for the manufacture of ceramic prototypes, parts with complex geometries, and large items. It is a simple, reliable, flexible, cost-effective and pollution-free process, but it requires an adequate understanding of colloidal suspensions and their behaviour. To produce high-quality sintered ceramic products, it is necessary to ensure the stability of the suspension, which determines the homogeneity of the suspension composition, and ensures the isotropic properties of the ceramic green body.

The second paper compares the morphology and mechanical properties (Vickers hardness, Vickers indentation fracture toughness and the indentation size effect using Vickers method and brittleness index) of cold isostatically pressed Al_2O_3 samples sintered by conventional (electrical) and non-conventional (hybrid microwave) techniques. The hybrid microwave heating was developed and used because the generated temperature field is distributed more evenly in the heated material, thus achieving uniform heating over the entire cross-section of the material and consequently avoiding the density gradient. By uniform heating, alumina ceramics with a more homogeneous and fine-grained microstructure and therefore improved final properties, can be obtained.

The last paper presents the study of the wear resistance of the slip cast monolithic and composite ceramics to solid particle erosion at different erodent (SiC) particles impact angles (30°, 60° and 90°) by measuring the erosion rate and surface roughness parameters. It was found that the erosion wear resistance of the monolithic alumina ceramics can be further improved by incorporating a small amount of zirconia (ZrO_2) particles in the alumina matrix in order to produce advanced Al_2O_3-ZrO_2 composite ceramics.

Guest-Editor
Lidija Ćurković, University of Zagreb, Faculty of Mechanical Engineering and Naval Architecture

CONTENT

Darko Landek, Lidija Ćurković, Ivana Gabelica, Irena Žmak, Zrinka Švagelj

Application of Simplex Lattice Mixture Design for Optimization of Rheological Properties of Alumina Suspensions for Slip Casting

[1] Faculty of Mechanical Engineering and Naval Architecture, University of Zagreb, Zagreb, Croatia

Abstract

In this work highly concentrated (70 wt. %) aqueous suspensions of alumina (Al_2O_3) were prepared for slip casting. The suspensions were stabilized with different combinations of three dispersants: (A) disodium salt monohydrate (Tiron), (B) Darvan C-N, 4,5-dihydroxy-1,3-benzenedisulfonic acid, and (C) citric acid monohydrate. The amounts of the dispersants were selected using the Simplex lattice mixture design to evaluate the effect of the dispersants content and their combination on the rheological properties of highly concentrated alumina suspensions. The regression analysis and the response surface plots showed a synergistic effect on decreasing the apparent suspension viscosity below 12 mPa·s, after the addition of small concentrations of the dispersants Tiron and the citric acid to the Darvan C-N. The antagonistic effect of the mixture of dispersants was obtained after adding small amounts of the Darvan C-N and citric acid to the Tiron, which increased the apparent viscosity up to 20 mPa·s.

Keywords: *alumina suspension, slip casting, viscosity, Simplex lattice mixture design.*

1. Introduction

Aluminium oxide or alumina (Al_2O_3) is an oxide technical ceramic material containing α-Al_2O_3 or corundum, the thermodynamically most stable form with the hexagonal unit cell (Figure 1). Also, alumina is available in various metastable polymorphs such as γ, δ, η, θ, κ, χ [1,2]. The oxygen anions (O^{2-}) define a nearly hexagonal close-packed (HCP) structure and the aluminium cations (Al^{3+}) occupy 2/3 of the octahedral sites in the HCP lattice. Each Al^{3+} centre is octahedral.

Among the ceramic materials, alumina is the most commonly used oxide ceramic due to its unique properties such as high elastic modulus, high wear resistance, high chemical corrosion resistance, high-temperature stability, retention of strength at high temperatures, but also brittleness and low fracture toughness [3]. Commonly, alumina is the first choice as a refractory material because of the low cost, simple handling and production, and the possibility to be shaped and sintered to full density without the use of protective atmosphere [4].

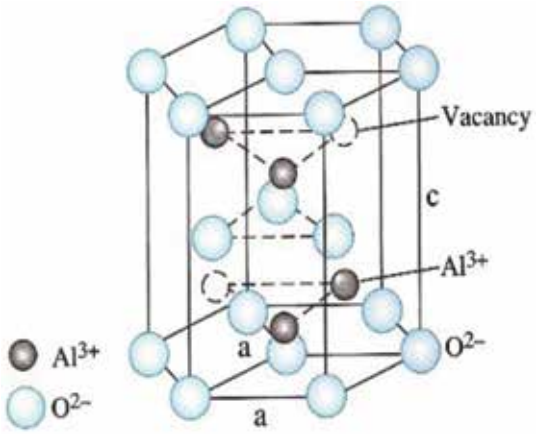

Fig. 1. Structure of α-Al_2O_3 [1].

Biocompatibility makes alumina a high-potential material in medical applications (dental, cardiologic, orthopaedic, bionic) [5,6]. High purity alumina (> 99.5 wt. %) may be used as a structural element and electric insulator

in nuclear reactors, for corrosion and wear protection, in automobile and spacecraft industry, in environmental industries, in water vapor processing, as well as in oil and gas energy production [6,7].

The selection of raw materials and additives, the forming of the green bodies, and the sintering process (conventional and non-conventional) together influence the formation of the vitally important microstructure, and thereby the desired properties of the final ceramic product (Figure 2) [8-10].

The methods for forming ceramic parts can be divided into the following basic types:

- pressing (0 – 15 % moisture)
- plastic forming (15 – 25 % moisture)
- casting (> 25 % moisture).

One of the simple forming casting methods is slip casting. It can be used for the manufacture of prototypes, parts with complex geometries as well as for large items.

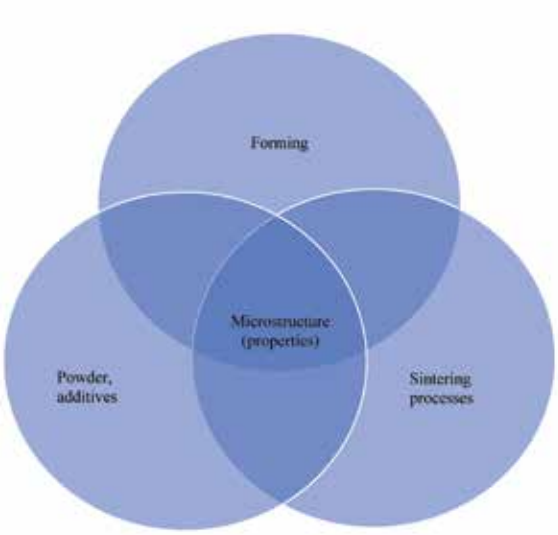

Fig. 2. Influences on microstructure and properties of ceramic parts.

The production of sintered products from slip cast alumina ceramics is carried out in three interdependent steps consisting of [11,12]:

(i) preparation of a stable suspension;
(ii) green body formation;
(iii) densification of the body during sintering.

To produce high-quality aluminium oxide ceramics by slip casting, an Al_2O_3 powder with particle sizes between 1nm and 1 mm is used, which is mixed with water, dispersants, and additives to form a stable highly concentrated suspension (a slip). The slip casting method uses gypsum moulds in which the suspensions dry by absorbing water (Figure 3). To produce a high-quality sintered ceramic product, it is necessary to ensure the stability of the ceramic suspension, which determines the homogeneity of the composition and the isotropic properties of the green body. The stability of the suspension is disturbed by the adhesion of the grains to aggregates that fall to the bottom in the form of sediment or the lifting of the grain by hydromechanical buoyancy and the formation of a surface film. Both phenomena result in the appearance of inhomogeneous areas in the suspension composition and later to the formation of porosity and poorer properties of the sintered product. The application of the dispersants reduces the apparent viscosity of the suspensions with very high solid content and increases the suspension stability, which allows good filling of the mould and obtaining uniform formation of the green body [5,6,13].

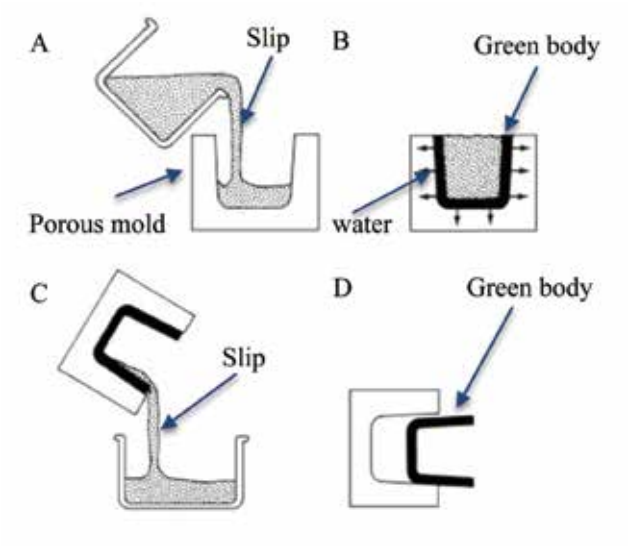

Fig 3. Schematic illustration of slip casting process: (A) filling a porous mould with slip, (B) removing water from suspension by capillary action through small pores in mould and formation of compact (green body) along mould walls, (C) draining excess slip, (D) green body drying and removing from mould [14].

The difference between the ceramic product obtained by slip casting a stable and an unstable suspension is best illustrated in Figure 4.

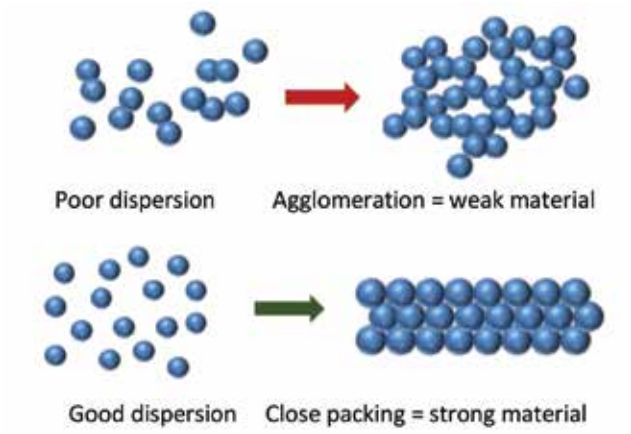

Fig. 4. Influence of particles dispersion on properties of sintered ceramic products [3].

The influence of the dispersant content and combination was investigated in several papers [15-17]. The usual industrial dispersants are ammonium polymethacrylate ("Darvan C-N") [18,19], 4,5-dihydroxy-1,3-benzenedisulfonic acid disodium salt ("Tiron") [20], poly(maleic acid) (PMA) [21] etc. It was found that the minimal viscosity (7 mPa·s) of highly concentrated alumina (70 wt. % of Al_2O_3 powder) water suspension was obtained with the addition of 0.75 wt. % of Darvan C-N, or 0.1 wt. % of Tiron or 0.3 wt. % of citric acid [5,6].

In this research, the influence of the combination of three dispersants Tiron (4,5-dihydroxy-1,3-benzenedisulfonic acid disodium salt monohydrate), Darvan C-N (an ammonium polymethacrylate water solution), and citric acid monohydrate on the viscosity of highly concentrated alumina suspensions for slip casting was investigated and statistically optimized.

2. Materials and methods

2.1. Preparation of alumina suspensions

Aqueous alumina suspensions with a solid loading of 70 wt. % were prepared from high purity Al_2O_3 powder (chemical composition of Al_2O_3 powder, according to the manufacturer's data, is given in Table 1) with an average particle size between 300 nm and 400 nm (Alcan Chemicals, Stamford, CT, USA), deionized water and three dispersants denoted as A, B, C:

- Dispersant "A" is 4,5-dihydroxy-1,3-benzenedisulfonic acid disodium salt monohydrate (Sigma-Aldrich Chemie GmbH, Germany) commercially named Tiron.

- Dispersant "B" is an ammonium polymethacrylate water solution (Vanderbilt Chemicals, LLC, CT, USA), commercially named Darvan C-N.

- Dispersant "C" is citric acid monohydrate, >99.7 % purity (VWR Chemicals, BDH Prolabo, Belgium).

Table 1. Chemical composition of Al_2O_3 powder.

Component, wt. %					
MgO	**Fe_2O_3**	**SiO_2**	**Na_2O**	**CaO**	**Al_2O_3**
0.066	0.015	0.02	0.05	0.013	balance

All suspensions were prepared by adding deionized water, dried ceramic powder, and dispersant into the grinding jar of a planetary ball mill. The grinding jar and ten balls used for the homogenization are made of alumina ceramics to prevent the contamination of suspensions. Each of the prepared suspensions was homogenized for 90 min at a rate of 300 rpm in the planetary ball mill (PM 100, Retsch, Germany). To remove air bubbles and to achieve homogeneity of the prepared suspensions, each suspension was treated in an ultrasonic bath.

2.2. Rheological measurements

Rheological measurements were conducted using the rotational viscometer DV-III Ultra (Brookfield Engineering Laboratories, Inc., MA, USA) in a small sample chamber with the SC4-18 spindle. Pre-shearing lasted for 2 min at a shear rate of 100 s^{-1}. The shear rate was gradually increased from 0.1 to 180 s^{-1}, and then reduced back to 0.1 s^{-1}. The shear rate increase/decrease interval was divided into 50 equal time frames of 3 seconds each. Rheological measurements were conducted just before each shear rate change. The temperature was kept constant at 25 °C ± 1 °C using the thermostatic bath Lauda EcoRE 415 (Lauda-Brinkmann, LP, USA). Flow curves were recorded for each dispersant type and each dispersant concentration.

2.3. Simplex lattice mixture design

The simplex lattice mixture design was used to evaluate the effect of different amounts of dispersants: Tiron (x_A), Darvan C-N (x_B), and citric acid (x_C) on the apparent viscosity of highly concentrated alumina suspensions. The concentrations of each dispersant in the 70 wt. % alumina suspensions were expressed as fractions of the mixture as shown in Figure 5.

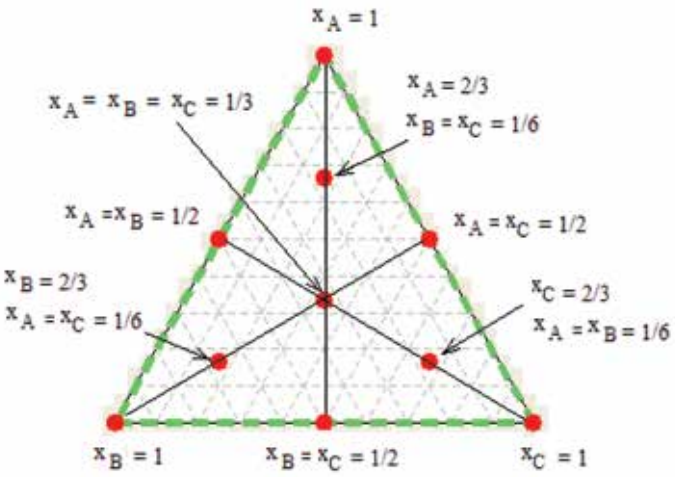

Fig. 5. Simplex lattice mixture test design for the addition of dispersants used in the preparation of 70 wt. % alumina suspensions.

The mixtures of dispersants were prepared as shown in Table 2. Three tested combinations were obtained with three single dispersants (label 1 to 3), three test combinations with two dispersants (label 5, 7, and 9), and four test combinations with three dispersant mixtures (label 4, 6, 8, and 10).

Table 2. Amounts of dispersants (Tiron, Darvan C-N and citric acid) in 70 wt. % alumina suspensions.

Label of suspension	Dispersant, wt. %		
	A: Tiron	B: Darvan C-N	C: citric acid
1	0.50	0	0
2	0	1	0
3	0	0	0.30
4	0.16	0.66	0.23
5	0.30	0	0.20
6	0.36	0.66	0.13
7	0.3	0.80	0
8	0.16	0.86	0.13
9	0	0.80	0.20
10	0.23	0.73	0.16

The experimental results of the apparent viscosity measurements were analysed using the MiniTab software, with a combination of response surface and regression analysis.

3. Results and discussion

3.1. Viscosity measurements

Viscosity measurements are often used to estimate suspension stability. The stability of highly concentrated alumina suspensions (70 wt. % Al_2O_3) was estimated by rheological measurements at a shear rate of 50 s^{-1}. This shear rate is usually achieved during gravity slip casting. The measured values of the apparent viscosity and pH values for the prepared suspensions are presented in Table 3. The lowest viscosities were obtained in suspensions 7 (0.3 wt. % Tiron, 0.8 wt. % Darvan C-N), 8 (0.16 wt. % Tiron, 0.86 wt. % Darvan C-N, 0.13 wt. % citric acid), and 9 (0.8 wt. % Darvan C-N, 0.2 wt. % citric acid). These results showed the synergistic effect of a combination of dispersants A + B, and A + B + C. The suspensions 1 and 5 showed the highest values of apparent viscosity and the antagonistic effect of the combination of dispersants A + C.

Table 3. Apparent viscosity and pH value of 70 wt. % Al_2O_3 suspensions with variation of added dispersants (shear rate 50 s^{-1}).

Label of test sample	pH	η, mPa·s
1	6.74	23.93
2	8.70	13.62
3	6.06	15.08
4	5.63	13.77
5	6.23	22.24
6	6.20	14.85
7	7.75	12.16
8	6.57	12.62
9	6.20	13.01
10	6.15	13.62

3.2. Statistical analysis

The contour plot of the response surface for measured apparent viscosity dependent on the dispersant content is shown in Figure 6. From the contour view of the measured apparent viscosity, the area of lower viscosity values is observed in the lower left-hand corner of the view. These favourable lower viscosity values are achieved by a combination of dispersants B (Darvan C-N) and C (citric acid), possibly with a small addition of dispersant A ($x_A < 1/3$).

The regression analysis of the response surface of apparent viscosity dependent on the type and content of dispersants was conducted using the MiniTab software. The influence of interactions among the dispersants Tiron (factor A), Darvan C-N (factor B), and citric acid (factor C) on the apparent viscosity is shown in Table 4.

Using the regression analysis and the results in Table 4 the following regression equation for the prediction of viscosity (η, mPa·s) of 70 wt. % alumina suspensions dependent on wt. % of added dispersants is estimated:

$$\eta = 23.42 \cdot x_A + 14.28 \cdot x_B + 15 \cdot x_C - 30.61 \cdot x_A \cdot x_B + \\ +5.32 \cdot x_A \cdot x_C - 8.66 \cdot x_B \cdot x_C \quad (1)$$

The coefficient of determination of the model in equation (1) is $R^2 = 0.9082$. The calculated regression model indicates a significant synergistic effect of the dispersants A and B on the reduction of suspension viscosity. This significance of an action is indicated by the p-value of their regression coefficient, which is 0.021 and satisfies the condition of statistical significance of the action of the observed effect in the experiment ($p < 0.05$), Table 4.

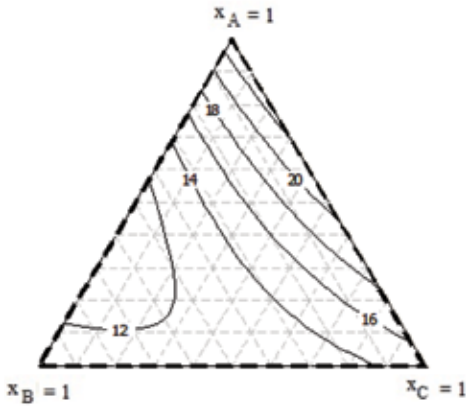

Fig. 6. Mixture contour plot of apparent viscosity (mPa·s) of the 70 wt. % alumina suspensions.

The estimated equation applies to the following concentrations of additives: Tiron from 0 to 0.50 wt. %, Darvan C-N from 0 to 0.86 wt. %, and citric acid from 0 to 0.30 wt. %, at ashear rate of 50 s^{-1}.

Mixing dispersants B and C also shows a synergistic effect on the reduction of viscosity, which can be deduced from the negative value of the regression coefficient with the product of their weight fractions. However, the combined effect of dispersants B and C on the viscosity reduction is not statistically significant, because the *p*-value of the product of their weight fractions is higher than 0.05. The antagonistic effect of the mixture of dispersants was obtained after adding small amounts of the Darvan C-N and the citric acid to the Tiron with increasing viscosity up to 20 mPa·s.

The addition of only one dispersant to the Al_2O_3 aqueous suspension reduces the viscosity of the suspension, but only for certain values of the weight fraction of the dispersant with small variations of the values around the optimal content. The simultaneous addition of two or three dispersants results in a reduction of the apparent viscosity with a wider allowable range of variation around the range of optimum dispersant proportions.

Table 4. Estimated regression coefficients in the linear model of apparent viscosity (η, mPa·s) of 70 wt. % alumina suspensions dependent on added dispersants.

Term	Coefficient	Sum of error of coef.	*p*-value
x_A	23.42	1.807	
x_B	14.28	1.807	
x_C	15.00	1.807	
$x_A \cdot x_B$	−30.61	8.326	0.021
$x_A \cdot x_C$	5.32	8.326	0.557
$x_B \cdot x_C$	−8.66	8.326	0.357

Based on equation (1) and Figure 5 the combination of dispersants can be optimized by looking for the combinations resulting in a minimum apparent viscosity of high-concentrated Al_2O_3 suspension suitable for slip-casting.

4. Conclusions

The focus of this research was on the influence of three different dispersants on the apparent viscosity of highly concentrated alumina suspensions with 70 wt. % of dry Al_2O_3 powder. The simplex lattice mixture design was used to evaluate the effect of different amounts of dispersants (Tiron, Darvan C-N, and citric acid) on viscosity. When analysing the rheological test results, the synergistic effect of decreasing the 70 wt. % alumina suspension viscosity was found for mixtures of dispersants Tiron and Darvan C-N (0.3 wt. % Tiron, 0.8 wt. % Darvan C-N), as well as for Darvan C-N and citric acid (0.8 wt. % Darvan C-N, 0.2 wt. % citric acid). The mixture of all three dispersants in the weight content: 0.16 wt. % Tiron, 0.86 wt. % Darvan C-N, and 0.13 wt. % citric acid also resulted in an acceptably low viscosity of the suspension. A linear regression model is proposed for the optimisation of the dispersant content, which is estimated on the basis of the statistical analysis of rheological measurements.

Acknowledgements

This work has been fully supported by the Croatian Science Foundation under the project IP-2016-06-6000: "Monolithic and composite advanced ceramics for wear and corrosion protection" (WECOR).

References

[1] Ćurković, L., Majić Renjo, M., Ciglar, D., Effects of cold isostatic pressing and granule size distribution on the densification of alumina ceramics. *Mater Test*, 57(6), 1–4 (2015).

[2] Greenwood, N.N., Earnshaw, A., Chemistry of the Elements. Oxford, Butterworth-Heinemann. (2012).

[3] Žmak, I., Ćorić, D., Mandić, V., Ćurković, L., Hardness and Indentation Fracture Toughness of Slip Cast Alumina and Alumina-Zirconia Ceramics. *Materials*, 13, 1–17 (2020).

[4] Gutiérrez, A.V., Cuevas, J.L., Ángeles, A.G., Pilalua, N., Addition of ceramics materials to improve the corrosion resistance of alumina refractories. *SN Applied Sciences*, 1(7), 1–7 (2019).

[5] Vukšić, M., Žmak, I., Ćurković, L., Ćorić, D., Effect of Additives on Stability of Alumina—Waste Alumina Suspension for Slip Casting: Optimization Using Box-Behnken Design. *Materials*, 12, 1–16 (2019).

[6] Sever, I., Žmak, I., Ćurković, L., & Švagelj, Z., Stabilization of highly concentrated alumina suspensions with different dispersants. *Transactions of FAMENA*, 3(72), 61–70 (2018).

[7] Ćurković, L., Kumić, I., Grilec, K., Solid particle erosion behaviour of high purity alumina ceramics, *Ceram Int*, 37, 29–35 (2011).

[8] Lóh, N.J., Simão, L., Jiusti, J., De Noni Jr., A., Montedo, O.R.K., Effect of temperature and holding time on the densification of alumina obtained by two-step sintering *Ceram Int*, 43(11), 8269–8275 (2017).

[9] Tian, Q., Dai, J., Xu, L., Wang, X., Advance of Sintering Methods of High Purity Alumina Ceramics. *Key Eng Mater*, 703, 76–80 (2016).

[10] Ćurković, L., Veseli, R., Gabelica, I., Žmak, I., Ropuš, I., Vukšić, M., A review of microwave-assisted sintering technique, *Transactions of Famena*, 45, 1–12 (2021).

[11] Landek, D., Ćurković, L., Gabelica, I, Kerolli Mustafa, M., Žmak, I., Optimization of Sintering Process of

Alumina Ceramics Using Response Surface Methodology, *Sustainability*, 13, 6739 (2021).

[12] Yuan, C.S., Wang, Z.J., Zhi, Q., Zhang, Y.M., Wang, X.D., Yang, J.F., The preparation and properties of alumina ceramics through a two-step pressureless sintering process, *Mater. Sci. Forum*, 922, 47–54 (2018).

[13] Boch, P., J Niepce, C., Ceramic Materials: Processes, Properties, and Applications., ISTE Ltd, London, UK, (2010).

[14] Souza, L.P.F., Mansur, H.S., Production and characterization of ceramic pieces obtained by slip casting using powder wastes, *J Mater Process Technol*, 145, 14–20 (2004).

[15] Tsetsekou, A., Agraotis, C., Milias, A., Optimization of the rheological properties of alumina slurries for ceramic processing applications Part I: Slip-casting, *J Eur Ceram Soc*, 21, 363-373 (2001).

[16] Majić Renjo, M., Lalić, M., Ćurković, L., Matijašić, G., Rheological properties of aqueous alumina suspensions, *Materwiss Werksttech*, 43, 979–983 (2012).

[17] Wu, L., Huang, Y., Liu, L. Meng, L., Interaction and stabilization of DMF-based alumina suspensions with citric acid, *Powder Technol*, 20, 477–481 (2010).

[18] Singh, B.P., Bhattacharjee, S., Besra, L., Sengupta, D.K., Evaluation of dispersibility of aqueous alumina suspension in presence of Darvan C, *Ceram Int*, 30(6), 939–946 (2004).

[19] Tsetsekou, A., Agrafiotis, C., Leon, I., Milias, A., Optimization of the rheological properties of alumina slurries for ceramic processing applications Part II: Spray-drying, *J Eur Ceram Soc*, 21(4), 493–506 (2004).

[20] Gulicovski, J.J., Čerović, L.S., Milonjić, S.K., Rheology of alumina suspensions stabilized with Tiron, *Korea Aust Rheol J*, 20(2), 65–71 (2008).

[21] Mohanty, S., Das, B., Dhara, S., Poly(maleic acid) - A novel dispersant for aqueous alumina slurry, *J Asian Ceram Soc*, 1(2), 184–190 (2013).

Lidija Ćurković[1], Ivana Ropuš[2], Irena Žmak[1], Ivana Gabelica[1], Zrinka Švagelj[1]

Comparison of Mechanical Properties of Conventionally and Non-Conventionally Sintered Cold Isostatically Pressed Al_2O_3 Ceramics

[1] Faculty of Mechanical Engineering and Naval Architecture, University of Zagreb, I. Lučića 1, 10000 Zagreb, Croatia
[2] Energoatest zaštita d.o.o., Potočnjakova 4, 10000 Zagreb, Croatia

Abstract

The objective of this study was to investigate and compare the morphology and mechanical properties of cold isostatically pressed (CIP) alumina (Al_2O_3) samples sintered by conventional (electrical) and non-conventional (hybrid microwave) techniques. Scanning electron microscopy (SEM) was used to examine the morphology of the Al_2O_3 ceramics sintered by both sintering techniques. Following mechanical properties of CIP alumina ceramics were analysed: (i) Vickers hardness, (ii) Vickers indentation fracture toughness (VIF), (iii) the indentation size effect (ISE) using Vickers method, and (iv) the brittleness index. The ISE is analysed using (i) the Meyer's law, (ii) the proportional specimen resistance (PSR) model, and (iii) the modified proportional specimen resistance (MPSR) model. It was found that alumina samples sintered in the electric kiln obtained higher density and lower porosity compared to the samples sintered in the hybrid-microwave kiln. The obtained values of the Meyer's index n are less than 2 for alumina ceramics sintered by both sintering methods, which indicates that the hardness is dependent on the test load. High correlation coefficients confirm that all applied mathematical models are suitable. However, true Vickers hardness obtained by the PSR model was found to be nearer to the measured Vickers hardness of alumina samples regardless of the sintering method applied. Furthermore, it was found that the fracture toughness was higher for alumina ceramics sintered in the hybrid microwave kiln (MK-Al_2O_3) than the one sintered in the electric kiln (EK-Al_2O_3). In contrary, the brittleness index was found to be higher for alumina ceramics sintered in the electric kiln (EK-Al_2O_3) than in the hybrid microwave kiln (MK-Al_2O_3). Both Vickers hardness and brittleness index values might be correlated to the microstructure of the sintered samples, e.g. finer for non-conventionally sintered alumina.

Keywords: *alumina ceramics, sintering, mechanical properties.*

1. Introduction

Each step of the ceramic production process: (i) the selection of raw materials and additives, (ii) the forming of the green bodies, and (iii) the sintering process have an important impact on the microstructure, and thereby the desired properties of the final ceramic product [1,2]. Sintering, as a final step in the ceramics production, may be conducted either by a conventional or non-conventional sintering method. The main goal of the sintering

process is to achieve full densification of the material, with the density as near as the theoretical density values as possible. Also, the sintering process can be used to obtain porous materials with high surface area. In this case, full consolidation is not reached.

The sintering of ceramic materials is an energy-consuming process with high production costs. To optimize the sintering process, densification mechanisms can be modified to improve the microstructure and mechanical properties of the obtained sintered ceramic materials as well as to reduce the production time and costs [1]. Therefore, emerging new techniques of sintering, such as spark plasma and microwave sintering are continuously being improved and applied. Microwave-assisted sintering, as one of the non-conventional sintering methods, was developed to reduce the energy consumption, maintain or improve the characteristics of the resulting ceramics, as well as to reduce the production costs and lessen environmental impact. With the microwave sintering method, highly dense materials can be obtained by rapid (>400 °C/min) and volumetric heating without substantial grain broadening because the processing times are considerably shorter than in conventional sintering [2,3]. The difference between the conventional and non-conventional sintering processes is in the heat transfer. Conventional sintering includes heat transfer via conduction from the outside to the inside of the sintered material, while the microwave heating process generates heat internally, i.e., within the sintered material and is transmitted outwards (Figure 1). The conventional sintering is based on conventional heat transfer mechanisms: conduction, convection, and radiation [3-5].

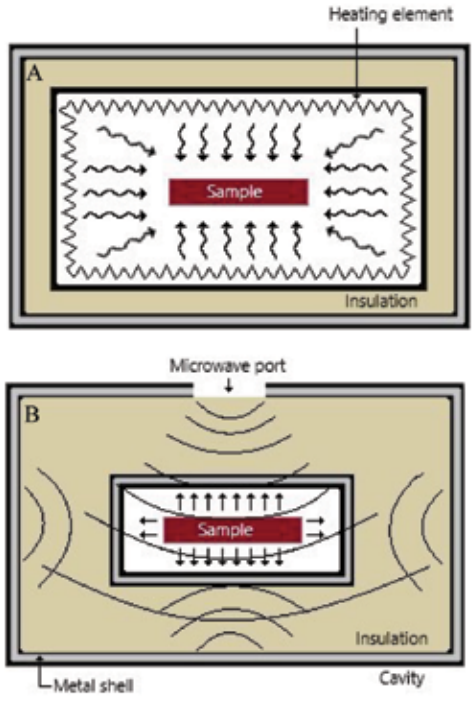

Fig. 1. Heating patterns in: (A) conventional furnace and (B) microwave furnace [4,5].

The interaction of microwaves with different materials depends on the electrical and magnetic properties of the material as well as on the grain size and porosity. Regarding these properties, materials can be classified as transparent (no energy transfer – low dielectric loss materials), opaque (no penetration into the material – bulk materials, conductors), and absorbent (absorption and exchange of energy – high dielectric loss materials), as shown in Figure 2.

Microwave sintering can be used for the preparation of different engineering materials: (i) ceramics, such as barium calcium zirconate titanate [7], magnesium aluminate spinel [8], yttria-tetragonal zirconia [9], high density yttria and lanthana co-doped zirconia dioxide [10], magnesium oxide doped alumina [11], Al_2O_3–yttria-stabilized ZrO_2 [12], alumina [13], β-SiC [14], (ii) metals and alloys, such as Ti-3Cu alloys [15], stainless steel 316L (X2CrNiMo17-12-2) [16], Cu–Sn bronze [17], FeCuCo metallic matrix [18], (iii) composites, for example Al_2O_3–SiC ceramic composites [19], W-30Cu composites [20], zirconia nanocomposite powders doped with ceria and toughened with alumina [21], boronised Ti6Al4V/HA composite [22], etc.

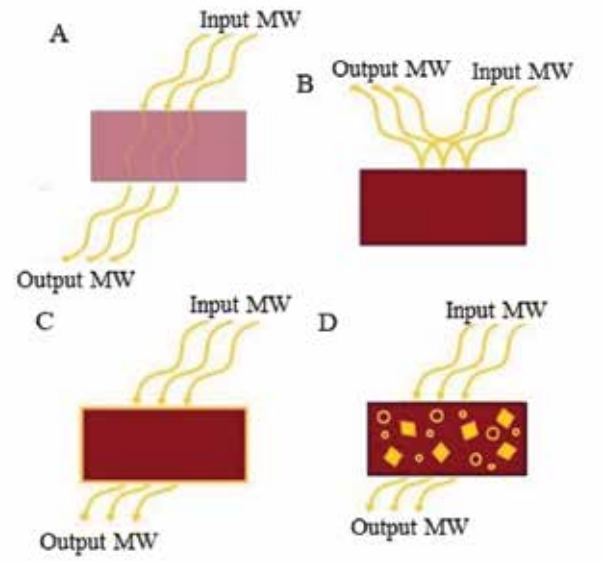

Fig. 2. Schematic diagram illustrating the interactions of microwaves with: (A) transparent material (low loss insulator) – total penetration, (B) opaque material (conductor) – no penetration, (C) absorber (lossy insulator) – partial to total penetration, and (D) absorber (mixed) –matrix is transparent, but fibres, particles or additives in matrix are absorbing materials – partial to total penetration [6].

Mechanical properties of the ceramic materials are strongly influenced by the degree of densification. Hardness, as one of the important mechanical properties of ceramic materials, represents material's resistance to plastic deformation. For testing very hard materials, such as ceramics, it is commonly used Vickers (*HV*) or Knoop (*HK*) method, because their diamond pyramidal penetrators can leave visible indentations. The value of

the applied load, used during the hardness testing, can influence the testing results [23]. The change in applied load causes changes in manifested ("apparent") hardness. The phenomenon when the hardness decreases with the increasing load (Meyer's number $n < 2$, Figure 3) is called normal indentation size effect (ISE) [24-28]. It is also possible that the material manifests an increase in hardness with increasing indentation load (Meyer's number $n > 2$, Figure 3), which is known as reverse ISE (RISE) [23,28,29]. Figure 3 illustrates non-constant or load dependent hardness ("apparent" hardness), and constant hardness ("true" hardness or load-independent hardness), which usually occurs at higher indentation loads [23,28].

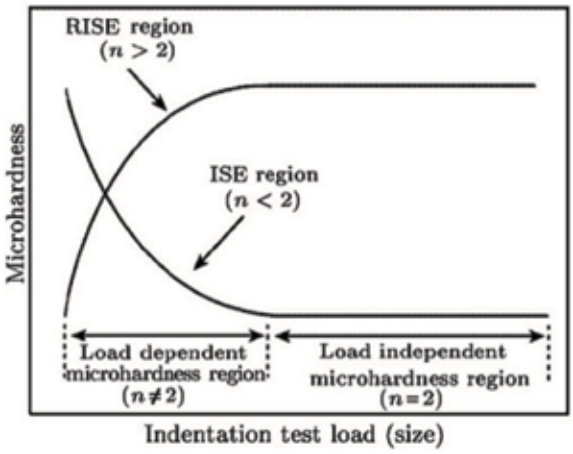

Fig. 3. Schematic plot of hardness variation with test load, showing the indentation size effect (ISE) and reverse indentation size effect (RISE) [23,28].

In this research, the morphology and the mechanical properties (Vickers hardness, Vickers indentation fracture toughness, the indentation size effect (ISE) using Vickers method, and the brittleness index) of cold isostatically pressed Al_2O_3 samples sintered by conventional (electric) and non-conventional (hybrid microwave) techniques were determined and compared. The observed ISE of alumina ceramics sintered in the electric and hybrid microwave kiln was analysed using the traditional Meyer's law, the proportional specimen resistance (PSR) model, and the modified proportional specimen resistance (MPSR) model.

Hybrid microwave heating was applied because the microwave-assisted sintered material distributes the temperature field more evenly, thus achieving a more uniform heating throughout the cross-section of the material (Figure 4) and, consequently avoiding the density gradient.

Due to this more uniform heating, alumina ceramics with a more homogeneous and fine-grained microstructure, and therefore improved final properties, can be obtained.

2. Materials and methods

High purity Al_2O_3 powder (Alteo, France) was used in this research as raw alumina powder for the preparation of alumina granules by spray drying. The chemical composition of the raw alumina powder according to manufacturer's declaration is listed in Table 1. According to the results of the chemical composition analysis, raw Al_2O_3 powder has a high purity of 99.83 wt. %. The presence of MgO as a sintering aid and the following impurities: CaO, Fe_2O_3, Na_2O and SiO_2 were also confirmed.

Table 1. Chemical composition of raw Al_2O_3 powder.

Sample	wt. %					
	CaO	Fe_2O_3	MgO	Na_2O	SiO_2	Al_2O_3
Al_2O_3 powder	0.0200	0.0180	0.0450	0.0500	0.0325	balance

Cold isostatic pressed (CIP) cylindrical pellets produced at Applied ceramics, Croatia, of high-purity Al_2O_3 ceramics with a diameter of 10 mm and a height of 20 mm were used in this research.

The cylindrical alumina pellets, used for the study of the conventional sintering method (samples "EK"), were sintered using an electric kiln (Nabertherm P310, Germany) at 1600 °C for 6 h. The second cylindrical pellet set (samples "MK") were sintered by the non-conventional sintering method in a hybrid microwave kiln (Over, Kerestinec, Croatia) at 1600 °C for 1 h. The sintering regimes were adopted according to the preliminary results [31].

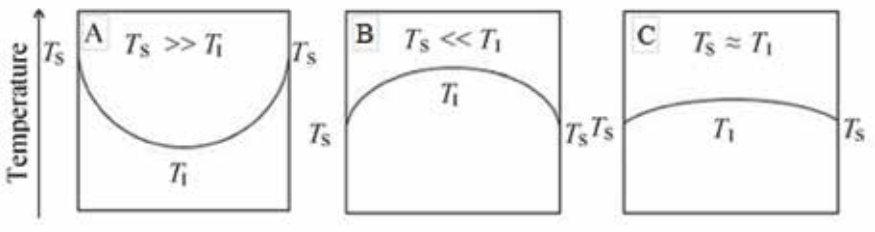

Fig. 4. Temperature distribution in ceramic material heated by: (A) conventional, (B) microwave, and (C) hybrid heating (T_s – surface temperature; T_I – internal temperature) [5,30].

The hybrid microwave kiln used a low-frequency (2.45 GHz) and 1.5 kW microwave magnetron. A silicon carbide susceptor was used to aid the heating of the sample in the microwave cavity.

The density of all sintered samples was determined according to the Archimedes' method using analytical balance Ohaus AP250D (Ohaus, Florham Park, NJ, USA).

The morphology of the fracture surface of the samples sintered by both techniques was analysed by the scanning electron microscope (SEM) TS5136LS (Tescan Vega, Brno, Czech Republic).

Prior to the measurements of Vickers hardness, the samples were prepared by the standard ceramographic technique [32]. Hardness tester Wilson Wolpert Tukon 2100B (*HV*0.1 – *HV*1) (Instron, Grove City, PA, USA) and Vickers tester Zwick (*HV*3 and *HV*5) were used for hardness measurement. Diagonals were measured on the optical microscope Olympus BH (Olympus Imaging Corp., Tokyo, Japan) immediately after unloading. The Vickers hardness was measured 10 times per sample under the loads listed in Table 2 at room temperature.

Table 2. Loads used for Vickers hardness testing.

F, N	*HV*
0.9807	*HV*0.1
2.942	*HV*0.3
4.903	*HV*0.5
9.807	*HV*1
29.42	*HV*3
49.03	*HV*5

The Vickers hardness was calculated according to the following equation [28]:

$$HV = \alpha \frac{F}{d^2} \quad (1)$$

where F stands for the applied load (N), d (mm) is the mean value of the indentation diagonals (Equation 2) [28], while α is the indenter's geometrical constant, i.e. 0.1891 for the Vickers diamond pyramid.

$$d = \frac{d_1 + d_2}{2} \quad (2)$$

Fracture toughness for alumina ceramics sintered by both sintering methods was determined by the Vickers indentation fracture (VIF) or Vickers indentation crack length method. This method uses the Vickers indenter to make the hardness indentation on a polished ceramic sample surface. The indenter creates a plastically deformed area underneath the indenter as well as cracks that emanate radially outward and downward from the vertices of the Vickers indentation.

Two types of cracks can occur: (i) radial-median cracks and (ii) Palmqvist cracks (Figure 5). A simple way to differentiate between the two types is to polish the surface layers away: the median crack system will always remain connected to the inverted pyramid of the indentation, while the Palmqvist cracks will become detached, as shown in Figure 5.

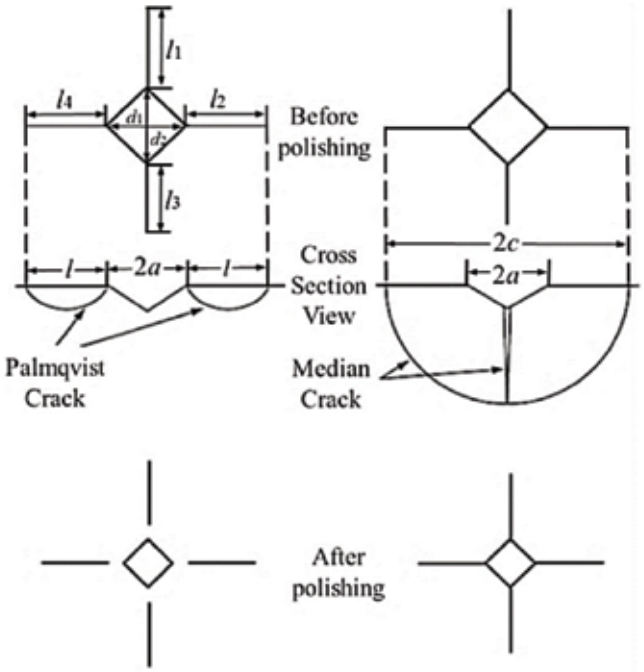

Fig. 5. Palmqvist and median crack system developed from the Vickers indents, before and after polishing [31].

A second way to distinguish the crack system present in the analysed material consists of the determination of *c/a* ratio (*c* is the crack length from the centre of the indent to the crack tip, and *a* is the half value of the indentation diagonal, Figure 5). If it is less than 2.5, then the material shows Palmqvist crack system, while for median cracks system values of *c/a* is higher than 2.5 [31]. The obtained values of *c/a* (for *HV*1) were 2.16 ± 0.26, and 1.81 ± 0.31 for alumina ceramics sintered in the electric and hybrid microwave kiln, respectively. The obtained values of *c/a* indicate that Palmqvist crack was present in both alumina ceramic samples. Therefore, three equations based on the Palmqvist crack were found to be applicable for the fracture toughness determination of the alumina ceramic samples (Table 3).

Table 3. Equations for the calculation of Vickers indentation fracture toughness (K_{IC}) values for Palmqvist crack type.

Equations	Authors
$K_{Ic} = 0.024 \cdot \frac{F}{c^{1.5}} \cdot \left(\frac{E}{HV}\right)^{0.5}$	Casellas [33]
$K_{Ic} = 0.0319 \cdot \frac{F}{a \cdot l^{0.5}}$	Shetty et al. [34]
$K_{Ic} = 0.0089 \cdot \left(\frac{E}{HV}\right)^{0.4} \cdot \frac{F}{a \cdot l^{0.5}}$ for $0.25 < l/a < 2.5$	Niihara et al. [34]

F, load applied during Vickers test (N); c, the crack length from the centre of the indentation to the crack tip (m); E, Young's modulus (GPa); HV, the Vickers hardness (GPa); l, the crack length measured from vertices of the indentation to the crack tip (m); a, half of the indentation diagonal (m).

3. Results and discussion

The SEM images of the microstructure of the ceramic fracture surface sintered by conventional (electric kiln) and non-conventional (hybrid microwave kiln) methods are shown in Figure 6.

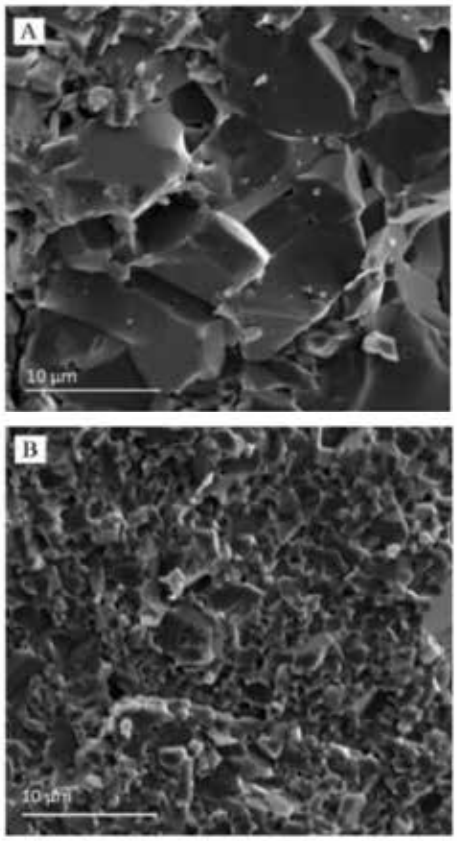

Fig. 6. SEM images of the fracture surface of Al_2O_3 ceramics sintered by (A) conventional (electric kiln) and (B) non-conventional (hybrid microwave kiln) sintering with the same magnification of 4500 times.

The most distinctive change was the grain size. Finer grain size was obtained for alumina samples sintered by the hybrid microwave kiln (non-conventional sintering method), where the process took less time and was more energy efficient.

The relative density of alumina ceramic sintered by conventional and non-conventional methods is 96.9 % ± 0.5 % and 94.9 % ± 0.7 %, respectively.

The porosity of alumina ceramic sintered by conventional and non-conventional methods is 3.1 % ± 0.5 % and 5.1 % ± 0.7 %, respectively.

The samples sintered in the electric kiln achieved a higher density and less porosity compared to the samples sintered in the hybrid-microwave kiln.

The value of Vickers hardness (HV) for different applied indentation load are presented in Figure 7.

The results show that the hardness decreases with the increasing indentation test load. The presented data on the dependence of the hardness on the applied load confirm the indentation size effect (ISE). The observed decrease in hardness with the increasing load is the normal ISE. All data shown in Figure are averages values of ten measurements.

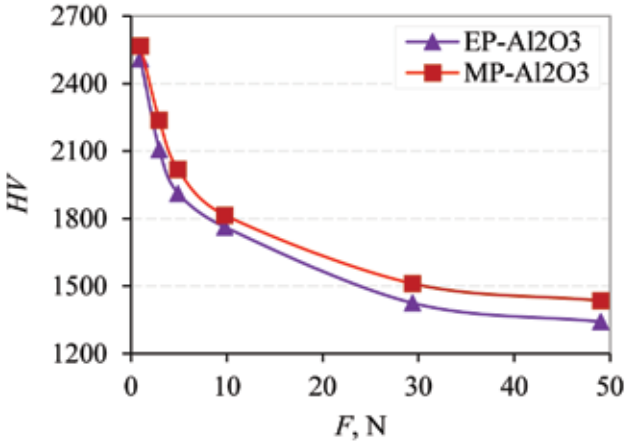

Fig. 7. Dependence of measured Vickers hardness on applied load for alumina ceramics sintered in (A) electric kiln (EK-Al_2O_3) and (B) hybrid microwave kiln (MK-Al_2O_3).

To quantify the normal indentation size effect (ISE), three models were applied to the obtained data: Meyer's law, the proportional specimen resistance (PSR) and the modified proportional specimen resistance (MPSR) model.

Meyer's law gives the relation between the applied load, F, and the average value of the indentation diagonals, d, according to Equation 3 [35].

$$F = K \cdot d^n \quad (3)$$

where n represents the Meyer's number (index), and K is the standard hardness constant for a given material. The

Equation 3 coefficients can be obtained by linear regression analysis from the log F versus log d plots (Figure 8), where the slope represents the Meyer's index, while the intercept gives log K values. These coefficients are shown in Figure 8 and listed in Table 4.

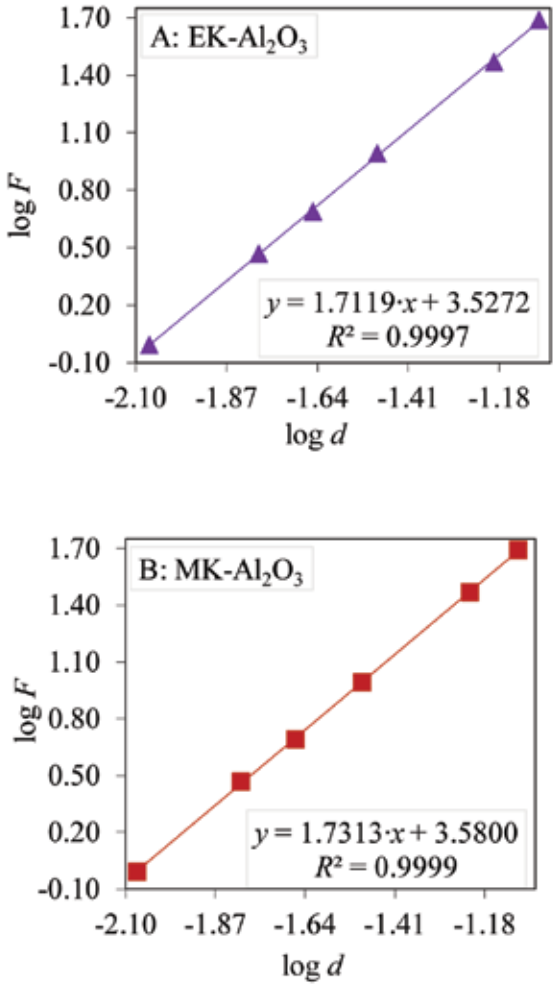

Fig. 8. Vickers hardness data for alumina ceramics sintered in (A) electric kiln (EK-Al_2O_3) and (B) hybrid microwave kiln (MK-Al_2O_3) according to Meyer's law

Table 4. Results of Vickers hardness data analysis according to Meyer's law for alumina ceramics sintered in the electric kiln (EK-Al_2O_3) and hybrid microwave kiln (MK-Al_2O_3).

Parameter	Sample	
	EK-Al_2O_3	MK-Al_2O_3
n	1.7119 ± 0.0228	1.7313 ± 0.0332
log K	3.5272 ± 0.0361	3.5800 ± 0.0526
K (N·mm^{-n})	2718	3619
R^2	0.9997	0.9999

The proportional specimen resistance (PSR) model is a modification of the Meyer's law [36], a modification that explains the relationship between the applied load, F, and the indentation diagonal, d, considering the energy balance. PSR is described by Equation 4:

$$F = a_1 \cdot d + a_2 \cdot d^2 \quad (4)$$

where a_1 (N·mm^{-1}) is a constant related to the specimen resistance representing the energy used to create new surfaces or the energy used in friction and elastic deformations. Coefficient a_2 (N·mm^{-2}) is a measure of the "true" hardness, meaning the hardness that is load independent and is related to permanent deformation [28,35]. These coefficients are shown in Figure 9 and listed in Table 5.

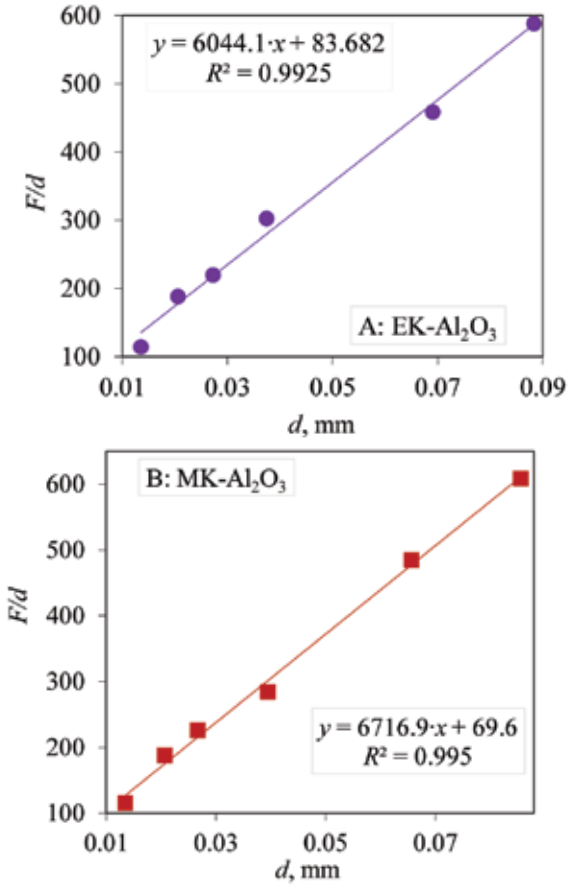

Fig. 9. Vickers hardness data for alumina ceramics sintered in (A) electric kiln (EK-Al_2O_3) and (B) hybrid microwave kiln (MK-Al_2O_3) according to proportional specimen resistance (PSR) model.

Modified proportional specimen resistance (MPSR) model is an expanded PSR model with an additional coefficient, a_0 (N) related to the material properties and the quality of sample surface preparation. MPSR model is expressed by Equation 5 [28,37].

$$F = a_0 + a_1 \cdot d + a_2 \cdot d^2 \quad (5)$$

The coefficients (a_2, a_1 and a_0.) of the obtained curves are presented in Table 6 and shown in Figure 10. The

coefficients obtained by polynomial regression analysis of the F versus d plot are presented in Table 6.

Table 5. Regression analysis results of experimental Vickers hardness data, according to proportional specimen resistance (PSR) model for alumina ceramics sintered in the electric kiln (EK-Al_2O_3), and hybrid microwave kiln (MK-Al_2O_3).

Parameter	Sample	
	EK-Al_2O_3	MK-Al_2O_3
a_1, N·mm^{-1}	83.7 ± 9.8872	69.9 ± 12.174
a_2, N·mm^{-2}	6044 ± 262	6717 ± 220
R^2	0.9925	0.9950

Table 6. Regression analysis results of experimental Vickers hardness data according to the modified proportional specimen resistance (MPSR) model for alumina ceramics sintered in (A) electric kiln (EK-Al_2O_3) and (B) hybrid microwave kiln (MK-Al_2O_3).

Parameter	Sample	
	EK-Al_2O_3	MK-Al_2O_3
a_0, N	0.058 ± 0.812	−0.019 ± 0.635
a_1, N·mm^{-1}	87 ± 49	72 ± 38
a_2, N·mm^{-2}	5963 ± 518	6691 ± 421
R^2	0.999	0.999

The residual surface stress coefficients a_0 reach relatively small values due to the careful grinding and polishing of the specimens.

"True" Vickers hardness HV_T can be calculated according to Equation 6 [28,37]:

$$HV_T = \alpha \cdot a_2 \quad (6)$$

where α is the geometrical constant of the indenter (0.1891 for Vickers), and a_2 is the coefficient of the PSR and MPSR models, related to the occurred permanent deformation. "True" Vickers hardness values of the sintered Al_2O_3 ceramics in the electric and hybrid microwave kiln are summarized in Table 7.

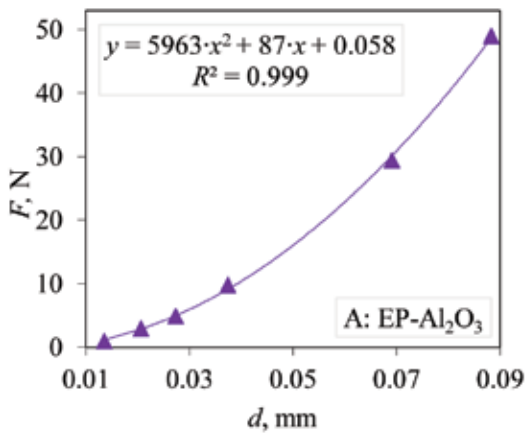

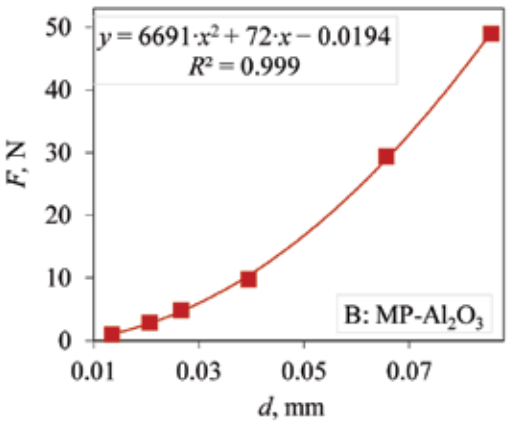

Fig. 10. The Vickers hardness data for alumina ceramics sintered in (A) electric kiln (EK-Al_2O_3) and (B) hybrid microwave kiln (MK-Al_2O_3) according to the modified proportional specimen resistance (MPSR) model.

Table 7. "True" Vickers hardness values of alumina ceramics sintered in the electric kiln (EK-Al_2O_3) and hybrid microwave kiln (MK-Al_2O_3), according to PSR and MPSR models.

Model	Sample	
	EK-Al_2O_3	MK-Al_2O_3
PSR	1143	1270
MPSR	1128	1265

The "true" values determined by PSR and MPSR models show an 11 % to 12 % higher hardness of the samples sintered in the hybrid microwave kiln (MK-Al_2O_3), compared to the samples sintered in the electric kiln (EK-Al_2O_3).

After measuring the alumina ceramics hardness by the Vickers indentation method, the lengths of cracks induced in the process were used to calculate the Vickers indentation fracture toughness (K_{Ic}) according to three chosen models (Table 3) for the Palmqvist crack type. The obtained results of the Vickers indentation fracture toughness for both alumina samples are presented in Figure 11.

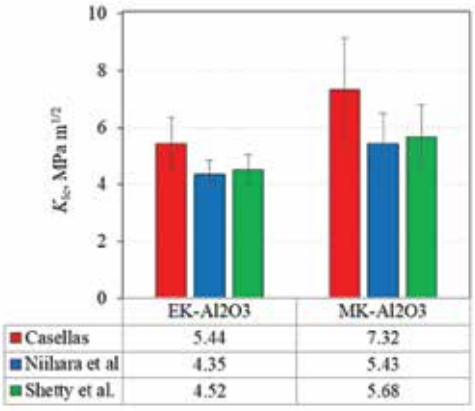

Fig. 11. Comparison of Vickers indentation fracture toughness values for alumina ceramics sintered in the electric kiln (EK-Al_2O_3), and (B) hybrid microwave kiln (MK-Al_2O_3) for Palmqvist crack type.

All applied models showed that the fracture toughness is higher for alumina ceramics sintered in the hybrid microwave kiln (MK-Al_2O_3) than in the electric kiln (EK-Al_2O_3).

For both alumina samples, the brittleness index (B_i, $\mu m^{-1/2}$) was calculated by the ratio of Vickers hardness ($HV1$, GPa), and the Vickers indentation fracture toughness (K_{IC}, $MPa \cdot m^{1/2}$) using the following equation [31,39]:

$$B_i = \frac{HV}{K_{IC}} \quad (7)$$

The calculated values of the brittleness index (B_i, $\mu m^{-1/2}$) for both sintered samples are shown in Figure 12. All models showed that the value of brittleness index is higher for alumina ceramics sintered in the electric kiln (EK-Al_2O_3) than in the hybrid microwave kiln (MK-Al_2O_3).

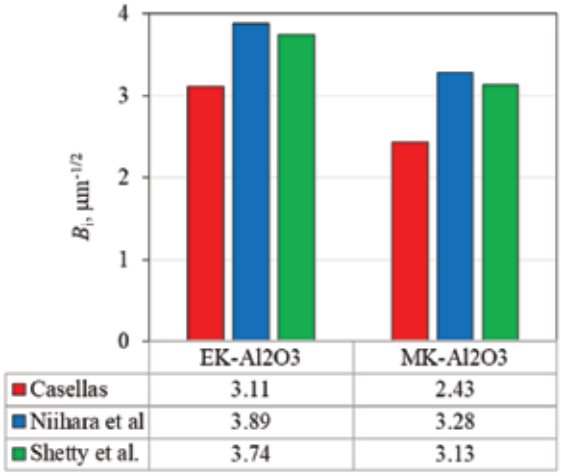

Fig. 12. Brittleness index (B_i, $\mu m^{-1/2}$) values for Palmqvist crack type.

4. Conclusions

The results presented in this paper may be summarized as follows:

- It was found that Al_2O_3 ceramics sintered in the electric kiln achieved a higher density and lower porosity, compared to the samples sintered in the hybrid-microwave kiln.
- The measured hardness of conventionally and non-conventionally sintered Al_2O_3 ceramics decreases with an increase in applied indentation load, meaning that both materials undergo the normal indentation size effect.
- Three different mathematical models were used for the analysis of the normal indentation size effect: the Meyer's law, the proportional specimen resistance (PSR) and the modified proportional specimen resistance (MPSR) model. Meyer's indexes were less than 2 for both samples: 1.7119 for the samples sintered in the electric kiln, and 1.7313 for the samples sintered in the hybrid microwave kiln, which also confirmed the normal indentation size effect.
- The samples sintered in the hybrid microwave kiln have a higher "true" Vickers hardness possibly due to the finer microstructure, compared to conventionally sintered alumina samples.
- The fracture toughness (K_{IC}, $MPa \cdot m^{1/2}$) is higher for alumina ceramics sintered in the hybrid microwave kiln (MK-Al_2O_3) than in the electric kiln (EK-Al_2O_3).
- The brittleness index (B_i, $\mu m^{-1/2}$) is higher for alumina ceramics sintered in the electric kiln (EK-Al_2O_3) than in the hybrid microwave kiln (MK-Al_2O_3).
- Both Vickers hardness and brittleness index values might be correlated to the microstructure of sintered samples.
- Non-conventionally sintered alumina samples have higher hardness and lower brittleness index probably due to the finer microstructure.

Acknowledgements

This work has been fully supported by the Croatian Science Foundation under the project IP-2016-06-6000: "Monolithic and composite advanced ceramics for wear and corrosion protection" (WECOR).

References

[1] Lóh, N.J., Simão, L., Jiusti, J., De Noni Jr., A., Montedo, O.R.K., Effect of temperature and holding time on the densification of alumina obtained by two-step sintering, *Ceram Int*, 43 (11), 8269–8275 (2017).

[2] Tian, Q., Dai, J., Xu, L., Wang, X., Advance of Sintering Methods of High Purity Alumina Ceramics, *Key Engineering Materials*, 703, 76–80 (2016).

[3] Figiel, P., Rozmus, M., Smuk, B., Properties of alumina ceramics obtained by conventional and non-conventional methods for sintering ceramics, *Journal of Achievements in Materials and Manufacturing Engineering*, 48 (1), 29–34 (2011).

[4] Agrawal, D., Microwave sintering of ceramics, composites and metal powders, in Sintering of Advanced Materials, Woodhead Publishing, 222–248 (2010).

[5] Ćurković, L., Veseli, R., Gabelica, I., Žmak, I., Ropuš, I., Vukšić, M., A review of microwave-assisted sintering technique, *Transactions of Famena*, 45, 1–12 (2021).

[6] Borrell, A., Salvador, MD., Advanced Ceramic Materials Sintered by Microwave Technology, In: IntechOpen., 2018.

[7] Orlik, K., Lorgouilloux, Y., Marchet, P., Thuault, A., Rguiti, M., Courtois, C., Jean, F., Influence of microwave sintering on electrical properties of BCTZ lead free piezoelectric ceramics, *J Eur Ceram Soc*, 40(4), 1212–1216 (2020).

[8] Liu, Y., Zhu, J., Dai, B., Transparent $MgAl_2O_4$ ceramics prepared by microwave sintering and hot isostatic pressing, *Ceram Int*, 46(16), 25738–25740 (2020).

[9] Ramesh, S., Zulkifli, N., Tan, CY., Wong, Y.H., Tarlochan, F., Ramesh, S., Teng, W.D., Sopyan, I., Bang, L.T., Sarhan, A.A.D., Comparison between microwave and conventional sintering on the properties and microstructural evolution of tetragonal zirconia, *Ceram Int*, 44(8), 8922–8927 (2018).

[10] Chen, Y., Fan, B., Yang, B., Ma, W., Liu, G., Li, H., Microwave sintering and fracture behavior of zirconia ceramics, *Ceram Int*, 45(14), 17675–17680 (2019).

[11] Croquesel, J., Carry, CP., Chaix, JM., Bouvard, D., Saunier, S., Direct microwave sintering of alumina in a single mode cavity: Magnesium doping effects, *J Eur Ceram Soc*, 38(4), 1841–1845 (2018).

[12] Shukla, M., Ghosh, S., Dandapat, N., Mandal, AK., Balla, VK., Comparative Study on Conventional Sintering with Microwave Sintering and Vacuum Sintering of Y_2O_2-Al_2O_3-ZrO_2 Ceramics, *Journal of Materials Science and Chemical Engineering*, 4(2), 71–78 (2016).

[13] Curto, H., Thuault, A., Jean, F., Violier, M., Dupont, V., Hornez, J.H., Leriche, A., Coupling additive manufacturing and microwave sintering: A fast processing route of alumina ceramics, *J Eur Ceram Soc*, 40(7), 2548-2554 (2020).

[14] Zhan, H., Zhang, N., Wu, D., Wu, Z., Bi, S., Ma., B, Liu, W., Controlled synthesis of β-SiC with a novel microwave sintering method, *Materials Letters*, 25, 126586 (2019).

[15] Tao, S.C., Xu, J.L., Yuan, L., Luo, J.M., Zheng, YF., Microstructure, mechanical properties and antibacterial properties of the microwave sintered porous Ti–3Cu alloys, *J Alloys Compd*, 812, 1–9 (2020).

[16] Nagaraju, K.V.V., Kumaran, S., Srinivasa Rao, T., Microwave sintering of 316L stainless steel: Influence of sintering temperature and time, *Materials Today: Proceedings*, 27(3), 2066–2071 (2020).

[17] Sethi, G., Upadhyaya, A., Agrawal, D., Microwave and Conventional Sintering of Premixed and Prealloyed Cu-12Sn Bronze, *Science of sintering*, 35, 49–65 (2003).

[18] Wang, L., Guo, S., Gao, J. et al., Microwave sintering behavior of FeCuCo based metallic powder for diamond alloy tool bit, *J Alloys Compd*, 727, 94–99 (2017).

[19] Madhan, M., Prabhakaran, G., Microwave versus conventional sintering: Microstructure and mechanical properties of Al_2O_3-SiC ceramic composites, *Boletin de la Sociedad Espanola de Ceramica y Vidrio*, 58(1), 14–22 (2019).

[20] Wei, C., Xu, X., Wei, B., Cheng, J., Chen, P., Effect of diamond surface treatment on microstructure and thermal conductivity of diamond/W-30Cu composites prepared by microwave sintering, *Diamond and Related Materials*, 104, 107760 (2020).

[21] Gil-Flores, L., Salvador, MD., Penaranda-Foix, FL. et al., Microstructure and mechanical properties of 5.8 GHz microwave-sintered ZrO_2/Al_2O_3 ceramics, *Ceram Int*, 45(14), 18059–18064 (2019).

[22] Peng, Q., Tang, Z., Wang, Y., Peng, Z., Mechanical performance and in-vitro biological behaviors of boronized Ti6Al4V/HA composites synthesized by microwave sintering, *Ceram Int*, 45(18), 24684–24690 (2019).

[23] Ćurković, L., Lalić, M., Šolić, S., Analysis of the indentation size effect on the hardness of alumina ceramics using different models, *Kov Mater*, 47 (2) 89–93 (2009).

[24] Bhattacharya, S., Kundu, R., Bhattacharya, K., Poddar, A., Roy, D. Micromechanical hardness study and the effect of reverse indentation size on heat-treated silver doped zinc-molybdate glass nanocomposites, *J Alloys Compd*, 770, 136–142 (2019).

[25] Kampouris, A.K., Konstantinidis, A.A., On the interpretation of the indentation size effect (ISE) through gradient theory for Vickers and Berkovich, *Journal of the Mechanical Behavior of Materials*, 25 (5–6), 161–164 (2017).

[26] Pharr, G.M., Herbert, E.G., Gao, Y., The indentation size effect: A critical examination of experimental observations and mechanistic interpretations, *Annual Review of Materials Research*, 40, 271–292 (2010).

[27] Peng, Z., Gong, J., Miao, H., On the description of indentation size effect in hardness testing for ceramics: Analysis of the nanoindentation data, *J Eur Ceram Soc*, 24, 2193–2201 (2004).

[28] Majić Renjo, M., Ćurković, L., Štefančić, S., Ćorić, D., Indentation size effect of Y-TZP dental ceramics. *Dent Mater*, 30 (12), e371–e376 (2014).

[29] Majić Renjo, M., Rede, V., Ćurković, L., Reverse indentation size effect of a duplex steel, Kov Mater, 52(5), 299-304 (2014).

[30] Menezes, R.R., Souto P.M., Kiminami, R.H.G.A., Microwave Fast Sintering of Ceramic Materials, In book: Sintering of Ceramics - New Emerging Techniques Edited by Arunachalam Lakshmanan, IntechOpen, 2012.

[31] Žmak, I., Ćorić, D., Mandić, V., Ćurković, L., Hardness and Indentation Fracture Toughness of Slip Cast Alumina and Alumina-Zirconia Ceramics, *Materials*, 13, 1–17 (2020).

[32] Chinn RE., Ceramography, Preparation and Analysis of Ceramic Microstructure. Materials Park: ASM International, 2002.

[33] Moraes, M.C.C., Elias, C.N., Mechanical properties of alumina-zirconia composites for ceramic abutments, *Mat Res*, 7(4), 643–649 (2004).

[34] Gong, J., Wu, J., Guan, Z., Analysis of the indentation size effect on the apparent hardness for ceramics, *Materials Letters*, 38, 197–201 (1999).

[36] Li, H., Bradt, R.C., The microhardness indentation load/size effect in rutile and cassiterite single crystals, *J Mater Sci*, 28, 917–926 (1993).

[37] Gong. J., Guan. Z., Load dependence of low-load Knoophardness in ceramics: a modified PSR model. *Mater Lett*, 47, 140–144 (2001).

[38] Montgomery, D.C. Design and Analysis of Experiments. John Wiley & Sons, Inc., 2013.

[39] Elsaka, S.E., Elnaghy, A.M., Mechanical properties of zirconia reinforced lithium silicate glass-ceramic, *Dent Mater*, 32, 908–914 (2016).

Lidija Ćurković[1], Zrinka Švagelj[1], Krešimir Grilec[1], Gorana Baršić[1], Vilko Mandić[2], Irena Žmak[1], Ivana Gabelica[1]

Comparison of Erosion Rate of Slip Cast Monolithic and Composite Ceramics

[1] Faculty of Mechanical Engineering and Naval Architecture, University of Zagreb, Zagreb, Croatia
[2] Faculty of Chemical Engineering and Technology, University of Zagreb, Zagreb, Croatia

Abstract

In this paper, the solid particle erosion wear of slip cast monolithic alumina (Al_2O_3) and alumina–zirconia (Al_2O_3–ZrO_2) composite ceramics was investigated. Three groups of samples were prepared: (i) monolithic alumina (Al_2O_3); (ii) composite alumina–zirconia (Al_2O_3–ZrO_2) containing 99 wt. % Al_2O_3 and 1 wt. % ZrO_2 and (iii) composite alumina–zirconia (Al_2O_3–ZrO_2) containing 90 wt. % Al_2O_3 and 10 wt. % ZrO_2. X-ray diffraction and scanning electron microscopy (SEM) were used to investigate the phase composition, the crystallite size, and the morphology of the sintered monolithic and composite ceramic samples. The erosive wear behaviour was studied under different impact angles (30°, 60°, 90°) of silicon carbide (SiC) particles as erodent. Erosion mechanisms of all prepared ceramic samples were evaluated by measuring the surface roughness parameters (R_a, R_z, and R_{max}) and the erosion rate. The obtained results showed that the tribological properties of the monolithic Al_2O_3 can be improved with the addition of ZrO_2. It was found that the erosion resistance increases with the increasing amount of ZrO_2 in the composite Al_2O_3–ZrO_2 ceramics. It was found that ZrO_2 grains are homogenously distributed in the alumina matrix, zirconia grain size is smaller than alumina grains, and that the alumina grain size is reduced by the addition of zirconia.

Keywords: *slip casting, erosion rate, monolithic alumina, alumina–zirconia composite ceramics.*

1. Introduction

Ceramic materials are, in general, divided into conventional ceramics and advanced ceramics. The use of conventional ceramics is growing at a slow rate, and some of their branches even show a decreasing tendency, for example refractory materials. In contrast to the conventional ceramics, the market for advanced ceramics is large and continuously growing. The production of advanced ceramics is very important and is one of the branches with highest economic potential in the developed countries and has received a great deal of attention from many fields of the industry. The appropriate forming technology for green bodies is important to manufacture high-quality advanced ceramics. Slip casting is an old forming technique in the ceramic industry and a method for the preparation of homogeneous large green bodies with a complex shape. Conventionally, plaster and resin are used for slip casting moulds. Improvement in slip properties and forming technologies is the way to improve the reliability of advanced ceramics and to lower their cost. Therefore, a lot of effort is put into the development of low-cost technologies for complex ceramic components. The near-net-shape forming of advanced ceramics excite the greatest interest. The following forming processes are currently in the stage of commercialisation or development: pressure slip casting, freeze casting, powder injection moulding, tape casting/lamination, rapid prototyping, and colloidal processing of powders. The technologies based on the colloidal processing, such as slip casting, gel casting, electrophoretic casting, hydrolysis-assisted solidification, direct coagulation casting, etc. are of great interest due to their ability to reduce the critical defects which can occur during the manufacturing process [1-8].

Slip casting is the most adequate technology to produce complex ceramic components. It is a simple, reliable, flexible, cost-effective, and pollution-free procedure, but it requires an adequate understanding of colloid suspensions and their behaviour. This knowledge is crucial for the optimization of technologies to produce improved ceramic products, e.g., slip, gel, and centrifugal casting, injection moulding, and coating. The properties of ceramic products strongly depend on the size of ceramic powder particles: when particles are smaller, the sintering is better and, consequently, product properties are better, too. On the other hand, ceramic particles smaller than 1μm, in combination with high suspension concentration, increase the suspension viscosity. The increased suspension viscosity is a consequence of greater interaction among particles, which can lead to agglomeration or flocculation [1-8]. This particle interaction can be controlled with additives (dispersants). For a multi-component system, the selection of the

dispersants becomes more critical because it might be difficult to find a dispersant that is optimal for all used components (Figure 1).

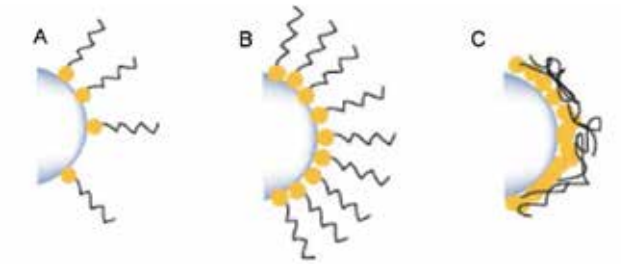

Fig. 1. Amount of additive: (A) too little, (B) optimal, (C) too much.

The particle interaction can be controlled with chemical additives in three different ways: electrostatic, steric, and electrosteric (a combination of the first two). The influence of additives (different dispersants) on the ceramic suspension stability has been extensively researched [1-8]. Despite that, the worldwide ceramic industry requires new, better additives to improve the slip casting process and, consequently, the ceramic products.

The slip casting process can be used for the manufacturing of monolithic and composite ceramic products of different sizes and shapes with homogeneous microstructure. In the past decade, several studies on rheological properties of binary systems, such as Al_2O_3–ZrO_2 composites, were performed [9-14]. For a multi-component system, the appropriate dispersant selection becomes more critical because it might be difficult to find a dispersant that is optimal for all used components. Slip casting of advanced ceramics based on alumina–zirconia requires the use of a dispersant, a binder, and an agent to prevent excessive grain growth. There are many commercially available dispersants and binders that can be used for the advanced ceramics slip casting process. However, the determination of a suitable combination and the quantification of optimal additions of the dispersant/binder pair with the starting particle size at the nano- and micro-levels can be time-consuming.

The suspension stability must be well achieved to establish complete control over suspension rheological properties. The sedimentation tests, the measurement of the zeta-potential and the apparent viscosity measurements are often used for the suspension stability estimation [3,10].

Aluminium oxide (Al_2O_3) or alumina, is an exceptionally important ceramic material and one of the most widely used advanced ceramics, which has many technological applications [2-4,15-18]. It has some extraordinary properties, like high hardness, chemical inertness, wear resistance and a high melting point. Because of their excellent properties, alumina ceramics are widely used for many refractory materials, grinding media, cutting tools and high temperature bearings. Therefore, a variety of mechanical parts and critical components used in chemical process environments, where materials are subjected to aggressive chemical atmosphere, extremely high temperatures and pressures, are typically made of alumina. Over the past thirteen years, several papers on corrosion [15,16,19,20], mechanical [10,17,21-24] and tribological [18,25-31] properties of advanced ceramics have been published. Industrial interest has been aroused as well, considering the broad array of advanced ceramic products for different applications, especially for tribological and corrosion applications.

Alumina ceramics (Al_2O_3) has the following properties: low fracture toughness (<5 MPa·m$^{1/2}$), low bending strength (<600 MPa) and high wear resistance. On the other side, yttria-stabilized tetragonal zirconia (t-ZrO_2) has high fracture toughness (6 MPa·m$^{1/2}$ to 15 MPa·m$^{1/2}$), high bending strength (1000 MPa to 1500 MPa) and high wear resistance. Mechanical and tribological properties of alumina can be improved by the addition of t-ZrO_2 (yttrium-stabilized tetragonal zirconia, Y-TZP). A disadvantage of pure zirconia is its low thermal conductivity compared to alumina: alumina has a thermal conductivity that is at least 3 times higher than that of zirconia. In a tribological contact, frictional heating occurs, and the low thermal conductivity of zirconia may cause thermally induced crack formation, followed by severe wear processes [10]. Improved properties of the monolithic alumina ceramics can be obtained by the incorporation of a small amount of zirconia (ZrO_2) particles in the alumina ceramic matrix to produce advanced Al_2O_3–ZrO_2 composite ceramics [10-14,30] (Figure 2).

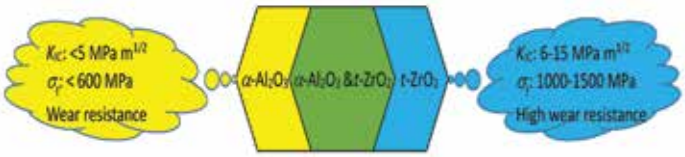

Fig. 2. Improved properties of alumina ceramics by addition of t-ZrO_2.

Erosion wear due to the flow of solid–liquid mixtures has shown dependence on many interrelated parameters: the properties of the target material, the present erodents and the carrier liquid are the major parameters affecting the material removal rate under similar flow conditions [32]. Solid particle erosion is the loss of material that results from repeated impacts of small, solid particles. In some cases, it is a useful phenomenon, as in sandblasting and high-speed abrasive waterjet cutting, but usually it is a serious problem in many engineering systems, including steam and jet turbines, pipelines and valves carrying particulate matter, and fluidized bed combustion systems. Solid particle erosion can occur in

a gaseous or liquid medium containing solid particles [33]. Erosive wear occurs by plastic deformation and/or brittle fracture, depending on the material being eroded and on the operating parameters. Ductile materials will wear by undergoing the process of plastic deformation, in which the material is removed by displacing or cutting by the eroding particles. In brittle materials, on the other hand, the material will be removed by the formation and intersection of cracks that radiate from the impact point of the eroding particles [34]. Ductile materials, such as pure metals, have the highest erosion rate at low angles of incidence (typically 15º to 30º), while for brittle materials the highest impact erosion rate usually occurs at 90º [33].

In this investigation, solid particle erosion tests were conducted to investigate the erosion wear behaviour of the slip cast monolithic high purity alumina and alumina–zirconia composite ceramics at different erodent particles impact angles at the room temperature. The erodent impact angles were 30°, 60° and 90°. Dry silicon carbide (SiC) was used as an erodent. Erosion mechanisms of all prepared ceramic samples were evaluated by measuring the erosion rate and roughness parameters (R_a, R_z, R_m).

2. Materials and methods

2.1. Preparation of green bodies of monolithic and composite ceramics by slip casting.

The green bodies of monolithic alumina (Al_2O_3) and alumina–zirconia (Al_2O_3–ZrO_2) composite ceramics were obtained by slip casting method. The first step in slip casting is the preparation of stable highly concentrated aqueous suspensions (the so-called "slips").

All suspensions contained 70 wt. % of dry ceramic powder and 30 wt. % of deionized water. The following components were used for the preparation of highly concentrated aqueous suspensions:

- high-purity α-Al_2O_3, with the average particle size of 300–400 nm (Alcan Chemicals, Stamford, CT, USA);
- high-purity t-ZrO_2 stabilized with 3 mol % of yttria (Y_2O_3), with the average particle size of 25 nm (SkySpring Nanomaterials Inc., Houston, TX, USA);
- an alkali-free anionic polyelectrolyte dispersant Dolapix CE 64 (Zschimmer & Schwarz GmbH & Co KG Chemische Fabriken, Lahnstein, Germany), with the molecule structure shown in Figure 3;
- 70 wt. % aqueous solution of the ammonium salt of polymethacrylic acid (PMAA–NH4);
- magnesium oxide added as magnesium aluminate spinel ($MgAl_2O_4$) made by Alfa Aesar, Haverhill, MA, USA, used to inhibit the abnormal alumina grain growth during the sintering process;
- deionized water.

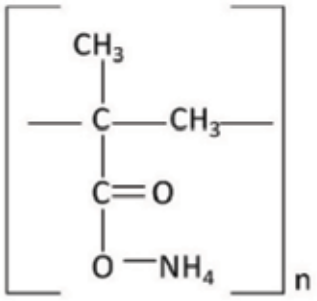

Fig. 3. The molecule structure of dispersant Dolapix CE 64.

Three groups of 70 wt. % alumina–zirconia aqueous suspensions (slips) were prepared:

- monolithic Al_2O_3 (composition: 100 wt. % Al_2O_3–0 wt. % ZrO_2);
- composite Al_2O_3–ZrO_2 ceramics (composition: 99 wt. % Al_2O_3–1 wt. % ZrO_2);
- composite Al_2O_3–ZrO_2 ceramics (composition: 90 wt. % Al_2O_3–10 wt. % ZrO_2).

The dispersant and the ceramic powders were added into the distilled water to form suspensions. They were homogenized for 90 min, at 300 rpm in the planetary ball mill (PM 100, Retsch GmbH, Germany). The grinding jar and balls used for homogenization were made of alumina as well to avoid sample contamination. Prior to the apparent viscosity measurement and forming of the green bodies, suspensions were ultrasonically treated in the ultrasonic bath BRANSONIC 220 (Branson Ultrasonics Corp., Danbury, CT, USA) with 50 kHz and 120 W to remove any trapped air bubbles and break down agglomerates.

The prepared suspensions were subjected to the rheological measurements on the rotational viscometer DV-III Ultra (Brookfield Engineering Laboratories, Inc., MA, USA) with a small sample chamber and spindle SC4-18. Samples were tempered at 25 °C ± 1 °C with the assistance of thermostatic bath Lauda Eco RE 415 (LAUDA-Brinkmann, LP, USA). Viscosity was determined at the shear rate of 50 s^{-1}, which is the exact shear rate of gravity slip casting.

2.2. Sintering of monolithic alumina and composite alumina–zirconia ceramics

Green bodies of monolithic Al_2O_3 and composite Al_2O_3–ZrO_2 ceramics were formed by the slip casting forming

method. After measuring the apparent viscosity, the suspensions with the minimum apparent viscosity were poured into previously prepared gypsum moulds and air-dried. The gypsum mould draws water from the poured slip and gives a form to the green body.

The prepared green bodies of monolithic Al_2O_3 and composite Al_2O_3–ZrO_2 ceramics were sintered by the conventional sintering in an electric kiln at 1650 °C, according to the sintering regime shown in Figure 4.

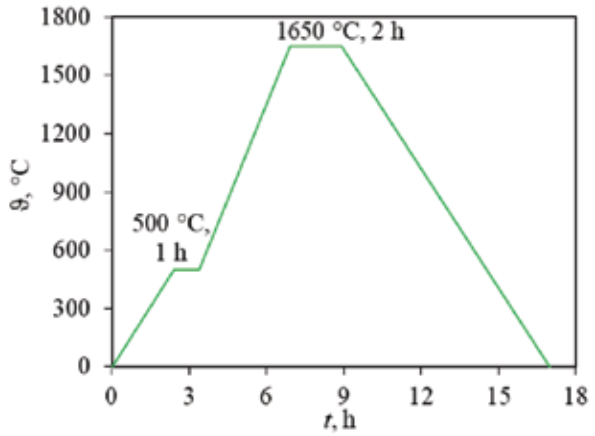

Fig. 4. Sintering regime of monolithic Al_2O and Al_2O_3–ZrO_2 composite ceramics.

Sintered samples (dimensions of 17 mm × 17 mm × 17 mm) of monolithic alumina and zirconia–alumina (with the addition of 1 and 10 wt. % ZrO_2) composite ceramics were prepared for the erosion tests by grinding and polishing, as per the standard ceramographic technique [35], to have a smooth surface finish. After polishing, the specimens were thoroughly ultrasonically cleaned in pure 94 vol. % alcohol and dried in a sterilizer at 150 ºC ± 5 ºC for 4 hours. The specimens were then annealed at 1200 °C for 360 min to eliminate any residual stresses that may have occurred during grinding and polishing.

2.3. Characterisation of monolithic and composite ceramics

Powder X-ray diffraction analysis (XRD) was used to investigate phase composition and crystallite size of monolithic and composite samples. XRD analysis was performed on XRD-6000 (Shimadzu, Tokyo, Japan) using CuKα radiation at an accelerating voltage of 40 kV and a current of 30 mA. All samples were analysed in a 2θ range of 5° to 75° in a continuous mode with a 0.02° 2θ step and a scan rate of 0.6 s.

The surface morphology of the sintered ceramic samples was determined by the scanning electron microscope (SEM), Tescan Vega Easy Probe 3, operating at 10 kV equipped with secondary (SE) and backscattered electron (BSE) detectors (Tescan, Brno, Czech Republic).

2.4. Erosion wear rate testing

The erosion test was carried out using an erosion testing apparatus (Figure 5), where samples were subjected to erosive wear of dry silicon carbide (SiC) particles as erodent.

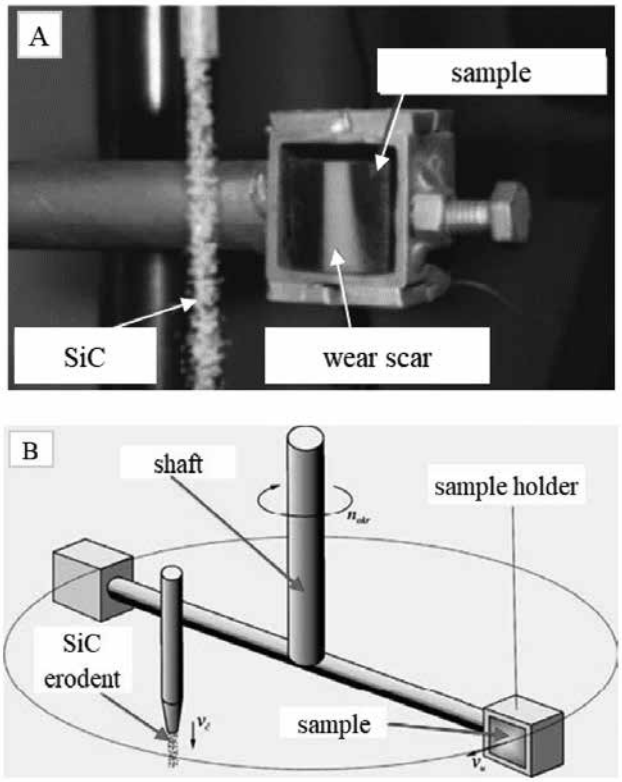

Fig. 5. (A) Sample holder in erosion test equipment, (B) scheme of sand equipment for erosion testing [18,25].

The erodent impact angles were 30°, 60° and 90°. When placed in the sample holders, the samples were span at about 1440 rpm through the seeping beam of the erodent powder. Two samples were eroded at the same time, one in each sample holder. The erodent powder was taken away by means of gravity and stored. Each test took 13 minutes and 53 seconds, to achieve approximately 20 000 impacts per sample and was carried out at room temperature. The erosion tests were repeated five times for each sample and each impact angle.

The abrasive particles properties are presented in Table 1 and the SEM micrograph of the used SiC erodent is shown in Figure 6. The SiC particles were sharp and angular, as seen in Figure 6.

Table 1. Properties of erodent particles: hardness (HV), density (ρ, kg/m^3), fracture toughness (K_{IC}, MPa·m$^{1/2}$).

Erodent	Average particle size, μm	HV	ρ, kg/m^3	K_{IC}, MPa·m$^{1/2}$
SiC	350	2800	3300	3.52

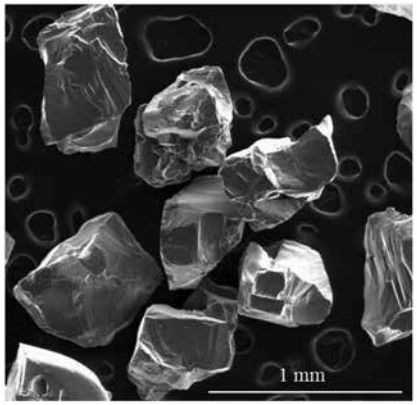

Fig. 6. SEM micrograph of erodent SiC particles.

The erosion mechanisms of all prepared ceramic samples were evaluated by measuring the following parameters before and after erosion:

- the surface roughness parameters (R_a, R_z, and R_{max});
- the erosion rates.

More precise information on erosion resistance was obtained by measuring the roughness parameters of the eroded surfaces. The roughness of each specimen was measured on five different tracing lanes using Perthometer S&P 4.5 (Feinprut Perthen GmbH, Göttingen, Germany). Before and after the erosion experiments, cleaned and dried samples of alumina ceramics were weighed in an electronic analytical balance to an accuracy of ± 0.01 mg. The amount of wear was determined by measuring the weight loss of ceramic samples (Δm).:

$$\Delta m = m_i - m_f \quad (1)$$

where m_i and m_f are the mass of the target material before and after the impact, respectively. The erosion rate is calculated using the weight loss approach [36]:

$$E = \frac{\Delta m}{m_e} = \frac{m_i - m_f}{m_e} \quad (2)$$

where E is the erosion rate (Δg/g), and me is the mass of the erodent.

3. Results and discussion

3.1. Apparent viscosity measurements

Apparent viscosity measurements were used for the suspension stability estimation. The suspension viscosity is at a minimum value when the dispersion of the ceramic particles is optimal. The rheological measurements showed that the measured apparent viscosity increases with the increasing zirconia content (Figure 7 and Table). The optimal amount of the dispersant Dolapix CE 64 also increases with the increasing zirconia content. The diagram in Figure 7 shows the apparent viscosity at a shear rate of app. 50 s^{-1}, which is the shear rate of the gravity slip casting.

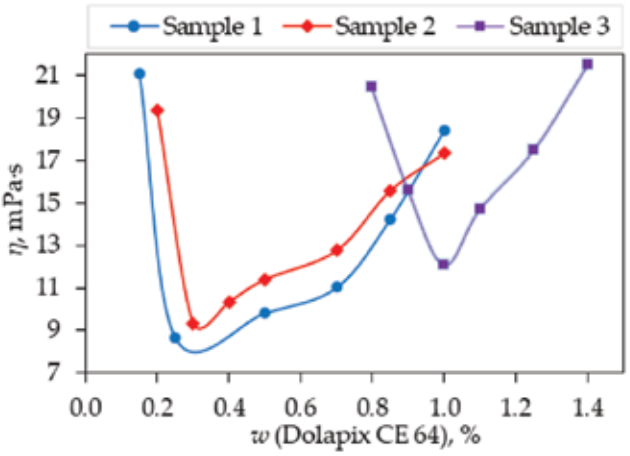

Fig. 7. Dependence of apparent viscosity on applied amount of Dolapix CE 64.

The compositions of all suspensions with the optimal amount of Dolapix CE 64 and the magnesium aluminate spinel are listed in Table 2.

Table 2. Compositions and apparent viscosity of 70 wt. % suspensions for slip casting of monolithic Al_2O_3 and Al_2O_3–ZrO_2 composite ceramics.

Suspension sample	**1**	**2**	**3**
wt. (Al_2O_3+ZrO_2), %	70	70	70
wt. (H_2O), %	30	30	30
wt. (Al_2O_3 in powder mixture), %	100	99	90
wt. (ZrO_2 in powder mixture), %	0	1	10
*wt.** (DOLAPIX CE 64), %	0.25	0.30	1.00
η, mPa·s	8.67	9.35	12.08

**wt.*, weight percent based on the dry ceramic powder

The optimal amounts of the dispersant and the magnesium aluminate spinel for each suspension were determined in previous research [10].

From the diffractogram in Figure 8, the qualitative phase composition was determined for all samples. The diffractogram indicates that the hexagonal Al_2O_3 consists of only α-Al_2O_3 crystalline phase (corundum) (ICDD PDF#46-1212). Qualitatively, sintered zirconia-toughened alumina composite shows the presence of α-Al_2O_3 (ICDD PDF#46-1212) as the main phase, t-ZrO_2 (ICDD PDF#42-1164) as the minor phase and m-ZrO_2 (ICDD PDF#37-1484) in traces. With an increase in the zirconia content, both t-ZrO_2 and m-ZrO_2 intensity

increased (the intensity increase of the t-ZrO_2 phase peak is highlighted).

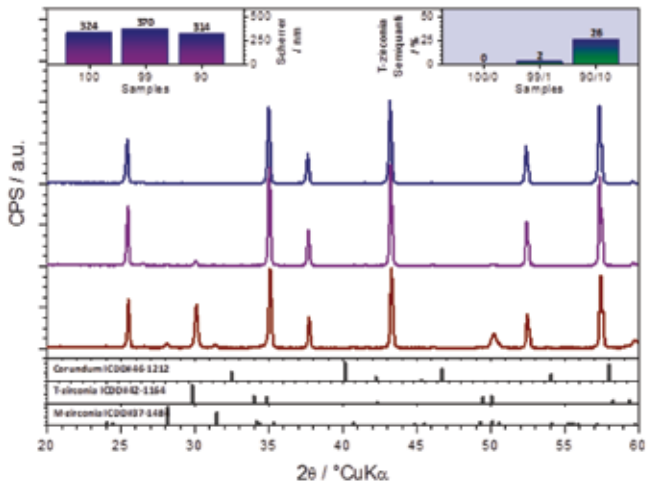

Fig. 8. Powder X-ray diffraction (XRD) results of monolithic Al_2O_3 (100 wt. % Al_2O_3), and Al_2O_3–ZrO_2 composite ceramics (1 wt. % ZrO_2 + 99 wt. % Al_2O_3 and 10 wt. % ZrO_2 +90 wt. % Al_2O_3).

The intensity of the t-ZrO_2 strongest peak and m-ZrO_2 strongest peak was compared to allow an insight into the mutual dependence of the zirconia phases (t-ZrO_2 to m-ZrO_2 ratio) as a function of the zirconia loading. With the introduction of 1 wt. % of zirconia, the relative content of the m-ZrO_2 was about 15 wt. % (i.e., 85 wt. % t-ZrO_2). However, the calculation of the ratio of zirconia phases that are present in total of about 1 wt. % in the analysed material may be questionable. Upon an increase in the zirconia loading to 10 wt. %, the relative presence of the m-ZrO_2 was reduced to about 7 wt. % (93 wt. % t-ZrO_2). As the microstructure is considered, the use of monolithic α-alumina yields crystallites of about 324 nm in size. Crystallite size was calculated by applying the Scherrer equation on the XRD patterns. Alumina crystallite size was increased to 370 nm by the addition 1 wt. % of zirconia to ceramic composites. The addition of 10 wt. % of zirconia to the composite reduced the crystallite size of alumina to 314 nm, thus favourably impacting the microstructure.

The results of the SEM analysis of the fracture surface of the sintered monolithic Al_2O_3 and Al_2O_3–ZrO_2 composite ceramics are shown in Figure 9. The ZrO_2 particles (the brighter phase) are distributed in the Al_2O_3 matrix, with some agglomerates of ZrO_2 and some pores.

The erosive wear behaviour of monolithic alumina and alumina–zirconia composite ceramics samples were evaluated by measuring:

- the roughness parameters (R_a, R_z, and R_{max});
- the erosion rate.

All measurements were made before and after the surface erosion of the investigated samples. SiC particles were used as erodent at impact angles of 30°, 60° and 90°.

The sintered samples were subjected to the solid particle erosion to determine whether the addition of the zirconia nanoparticles improves the erosion resistance of alumina. Solid particle erosion can be defined as a degradation of the material caused by repeated impacts of small solid particles [18,25,33,37]. According to the literature, the lower impact angle (30°) corresponds to the abrasive erosion, while the higher impact angle (90°) correlates with the impact erosion [18,25,33,37]. Wear mechanisms were analysed by comparing the surface roughness (microroughness) parameters before and after the erosion test using a profilometer. It is assumed that higher surface roughness after the test indicates lower erosion resistance [18,25].

Three main roughness parameters were obtained from this test:

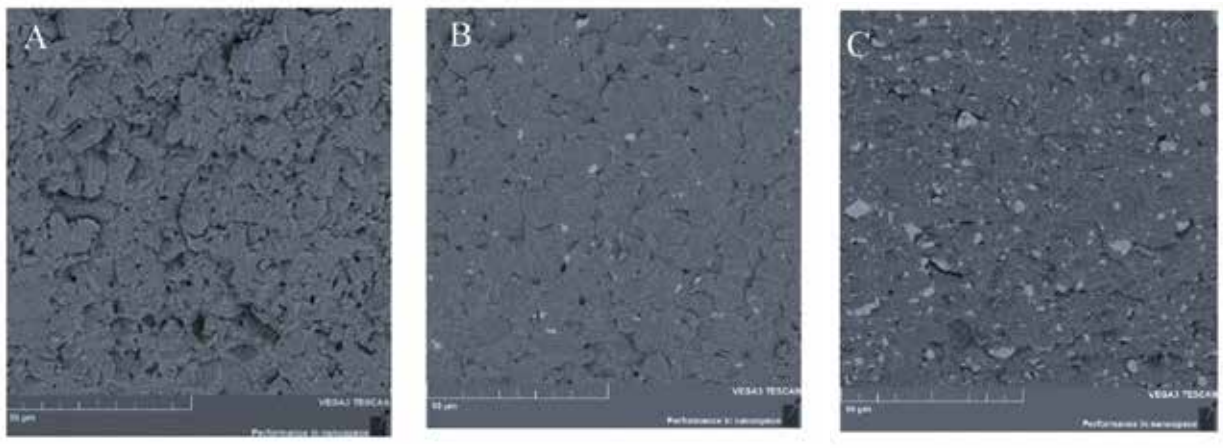

Fig. 9. SEM micrographs of fracture surface morphology of Al_2O_3–ZrO_2 composite ceramics with different ZrO_2 content: (A) 0 wt. %, (B) 1 wt. %, (C) 10 wt. %, prepared by slip casting and sintered at 1650 °C.

- R_a - the roughness average;

- R_z - the ten-point average of the profile;

- R_{max} - the maximum between the peak and the valley.

In Figure 10 the obtained values of the roughness parameters before and after erosion with SiC particles at 30°, 60° and 90° impact angles are presented. The roughness parameters (R_a, R_z, and R_{max}) are presented as mean values of five measurements and standard deviation ($\bar{x} \pm 2\,s$).

After the erosion test, all surface roughness parameters increased for all samples. The obtained results confirmed that these types of slip cast monolithic and composite ceramics are more sensitive to impact than to abrasive erosion, since all surface roughness parameters were higher for the higher impact angle (90°) for all samples, Figure 10.

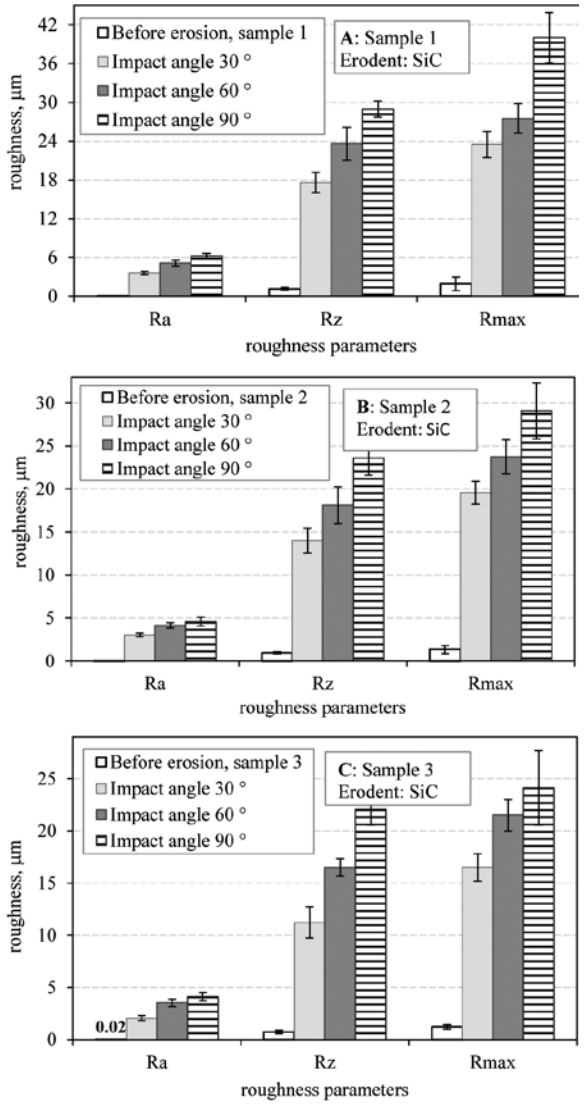

Fig. 10. Values of roughness parameters ($\bar{x} \pm 2\,s$) before and after erosion with SiC particles at 30°, 60° and 90° impact angles for (A) sample 1: 100 wt. % Al_2O_3, (B) sample 2: 99 wt. % Al_2O_3+1 wt. % ZrO_2, (C) sample 3: 90 wt. % Al_2O_3+10 wt. % ZrO_2.

This investigation also confirmed the hypothesis that the tribological properties of the alumina can be improved with the addition of zirconia nanoparticles: all surface roughness parameters were higher for the monolithic alumina than for the alumina–zirconia composites at all impact angles.

Figure 11 illustrates the erosion rates (mean value and standard deviation, $\bar{x} \pm 2\,s$) of alumina ceramics plotted against the impact angle. The erosion rate is determined according to equation 2. Tests were repeated five times for each experimental condition. The erosion wear tests for all ceramic samples were performed by SiC particles at impact angles of 30°, 60° and 90°. The obtained results indicate that both composite ceramics were more resistant to the impact erosion than monolithic alumina ceramics.

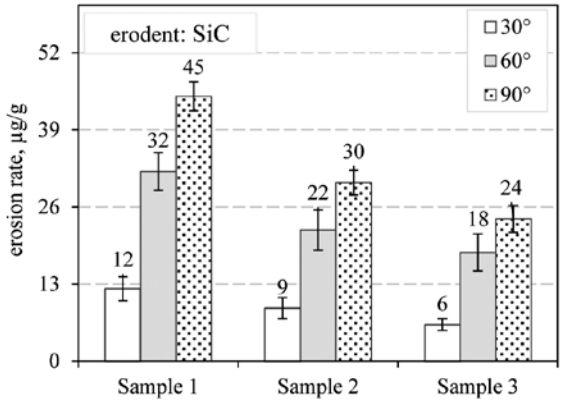

Fig. 11. Erosion rate ($\bar{x} \pm 2\,s$) after erosion with SiC particles at 30°, 60° and 90° impact angles for:
sample 1 (100 wt. % Al_2O_3),
sample 2 (99 wt. % Al_2O_3+1 wt. % ZrO_2) and
sample 3 (90 wt. % Al_2O_3+10 wt. % ZrO_2).

From the results presented in Figure 11 it is obvious that the erosion rates of all ceramic samples increase with increasing impact angle, with the maximum erosion rate occurring at an impact angle of 90°. Since the lower impact angle (30°) is related to the abrasive type of erosion, and the higher impact angle (90°) is related to the impact erosion, it can be concluded that all studied ceramic samples are more resistant to abrasive than to impact erosion.

4. Conclusions

The green bodies of the monolithic Al_2O_3 and composite Al_2O_3–ZrO_2 ceramics (composition: 99 wt. % Al_2O_3 + 1 wt. % ZrO_2, and 90 wt. % Al_2O_3 and 10 wt. % ZrO_2) were formed by the slip casting process in a plaster mould. After drying and green machining, green bodies were sintered at a temperature of 1600 °C.

SEM analysis of the prepared composite ceramics showed that the ZrO_2 particles are well dispersed in

Al_2O_3 matrix for both samples (containing 1 wt. % and 10 wt. % of ZrO_2), with some agglomerates of ZrO_2 and some pores. The relative presence of the m-ZrO_2 was found to be about 7 wt. % vs. 93 wt. % of t-ZrO_2 (for the sample with 10 wt. % ZrO_2).

Alumina crystallite size increased from 324 nm to 370 nm by the addition 1 wt. % of ZrO_2 to the ceramic composite. Conversely, the addition of 10 wt. % of ZrO_2 reduced the Al_2O_3 crystallite size to 314 nm.

The sintered samples were subjected to the erosion resistance test using the SiC particles under different impact angles (30°, 60°, 90°) and the following conclusions were drawn:

- Surface roughness parameters increased after erosion.
- All surface roughness parameters were higher for monolithic alumina than for zirconia–alumina composite ceramics.
- The erosion rate decreased with the increase of the ZrO_2 content in the alumina matrix.
- All ceramic samples were more sensitive to impact than to abrasive erosion.

Acknowledgements

This work has been fully supported by the Croatian Science Foundation under the project IP-2016-06-6000: “Monolithic and composite advanced ceramics for wear and corrosion protection” (WECOR).

References

[1] Wu, L., Huang, Y., Liu, L. Meng, Interaction and stabilization of DMF-based alumina suspensions with citric acid. Powder Technol, 203, 477–481 (2010).

[2] Vukšić, M., Žmak, I., Ćurković, L., Ćorić, D., Effect of Additives on Stability of Alumina—Waste Alumina Suspension for Slip Casting: Optimization Using Box-Behnken Design. Materials, 12, 1–16 (2019).

[3] Sever, I., Žmak, I., Ćurković, L., Švagelj, Z., Stabilization of highly concentrated alumina suspensions with different dispersants. Transactions of FAMENA, 3(72), 61–70 (2018).

[4] Landek, D., Ćurković, L., Gabelica, I, Kerolli Mustafa, M., Žmak, I., Optimization of Sintering Process of Alumina Ceramics Using Response Surface Methodology. Sustainability, 13, 6739 (2021).

[5] Mohanty, S., Das, B., Dhara, S., Poly(maleic acid) - A novel dispersant for aqueous alumina slurry. J Asian Ceram Soc, 1(2), 184–190 (2013).

[6] Majić Renjo, M., Lalić, M., Ćurković, L., Matijašić, G., Rheological properties of aqueous alumina suspensions. Mater Werkst, 43, 979–983 (2012).

[7] Tallon, C., Limacher, M., Franks, G.V., Effect of particle size on the shaping of ceramics by slip casting. J Eur Ceram Soc, 30, 2819–2826 (2010).

[8] Xu, Y., Mao, X., Fan, J., Li, X., Feng, M., Jiang, B., Lei, F., Zhang, L., Fabrication of transparent yttria ceramics by alcoholic slip-casting. Ceram Int, 43(12), 8839–8844 (2017).

[9] León-Carriedo, M., Gutiérrez-Chavarría, C.A., Rodríguez-Galicia, J.L., Multilayered Zircon-Alumina Components Fabricated by Slip Casting. Materials Science Forum, 755, 145–151 (2013).

[10] Žmak, I., Ćorić, D., Mandić, V., Ćurković, L., Hardness and Indentation Fracture Toughness of Slip Cast Alumina and Alumina-Zirconia Ceramics. Materials, 13, 1–17 (2020).

[11] Guimaraes, F.F.A.T., Silva, K.L., Trombini, V., Pierri, J.J., Rodrigues, J.A., Tomasi, R., Pallone, E.M.J.A., Correlation between microstructure and mechanical properties of Al_2O_3/ZrO_2 nanocomposites. Ceram Int, 35(2), 741–745(2009).

[12] Wakily, H., Mehrali, M., Metselaar, H.S.C., Preparation of Homogeneous Dense Composite of Zirconia and Alumina (ZTA) using Colloidal Filtration. World Academy of Science, Engineering and Technology, 46, 140–145 (2010).

[13] Sun, L., Sneller, A., Kwon, P., Fabrication of alumina/zirconia functionally graded material: From optimization of processing parameters to phenomenological constitutive models. Materials Science and Engineering A, 488, 31–38 (2008).

[14] Zhang, Y., Sun, M.J., Zhang, D., Designing functionally graded materials with superior load-bearing properties. Acta Biomaterialia, 8, 1101–1108 (2012).

[15] Ćurković, L., Fudurić Jelača, M., Kurajica, S., Corrosion behaviour of alumina ceramics in aqueous HCl and H_2SO_4 solutions. Corros Sci, 50, 872–878 (2008).

[16] Ćurković, L., Fudurić Jelača M., Dissolution of alumina ceramics in HCl aqueous solution. Ceram Int, 35, 2041–2045 (2009).

[17] Ćurković, L., Lalić, M., Šolić, S., Analysis of the indentation size effect on the hardness of alumina ceramics using different models. Kovove Materialy-Metallic Materials, 47, 89–93(2009).

[18] Ćurković, L., Kumić, I., Grilec, K., Solid particle erosion behaviour of high purity alumina ceramics. Ceram Inter, 57, 29–35(2011).

[19] Kurajica, S., Mandić, V., Ćurković, L., Mullite ceramics acid corrosion kinetics as a function of gel homogeneity, Biointerface Research in Applied Chemistry, 7(6), 2295–2299 (2017).

[20] Živko-Babić, J., Lisjak, D., Ćurković, L., Jakovac, M., Estimation of chemical resistance of dental ceramics by neural network. Dent Mater, 24, 18–27 (2008).

[21] Majić, M., Ćurković, L., Ćorić, D., Load dependence of the apparent Knoop hardness of SiC ceramics in a wide range of loads. Mater Werkst, 42, 234–238 (2011).

[22] Elsaka, S.E., Elnaghy, A.M., Mechanical properties of zirconia reinforced lithium silicate glass-ceramic. Dent Mater, 32, 908–914 (2016).

[23] Wan, W., Yang, J., Feng, Y., Bu, W., Qiu, T., Effect of trace alumina on mechanical, dielectric, and ablation properties of fused silica ceramics. J Alloys Compd, 675, 64–72 (2016).

[24] Bhattacharya, S., Kundu, R., Bhattacharya, K., Poddar, A., Roy, D., Micromechanical hardness study and the effect of reverse indentation size on heat-treated silver doped zinc-molybdate glass nanocomposites. J Alloys Compd, 770, 136–142 (2019).

[25] Grilec, K., Ćurković, L., Kumić, I., Baršić, G., Erosion mechanisms of aluminium nitride ceramics at different impact angles. Mater Werkst, 42, 712–717(2011).

[26] Celotta, D.W., Qureshi, U.A., Stepanov, E.V., Goulet, D.P., Hunter, J., Buckberry, C.H., Hill, R., Sherikar, S.V., Moshrefi-Torbati, M., Wood, R.J.K., Send erosion testing of novel composites and hard ceramics. Wear, 263, 278–283 (2007).

[27] Wu, T., Zhou, J., Wu, B., Xiong, Y., Effect of Y_2O_3 additives on the wet abrasion resistance of an alumina-based grinding medium. Wear, 356–357, 9–16 (2016).

[28] Wu, T., Zhou, J., Wu, B., Li, W., Effect of La_2O_3 content on wear resistance of alumina ceramics. Journal of Rare Earths, 34, 288–294 (2016).

[29] Pereira de Oliveira, R., Santos, E. dos, Cousseau, T., Sinatora, A., Effect of pH on wear and friction of silicon nitride sliding against alumina in water. Tribol Int, 90, 356–361(2015).

[30] Pulgarin, H.L.C., Garrido, L.B., Albano, M.P., Comparison of different zirconia powders for slip casting of alumina–zirconia ceramics. Advances in Applied Ceramics, 12, 39–45 (2013).

[31] Milak P.C., Minatto F.D., De Noni Jr. A., Montedo O.R.K., Wear performance of alumina-based ceramics - a review of the influence of microstructure on erosive wear. Ceramica, 61, 88–103 (2015).

[32] Desale G.R, Gandhi B.K., Jain S.C., Effect of erodent properties on erosion wear of ductile type materials. Wear, 261, 914–921 (2006).

[33] SM SM Handbook, Friction, lubrication, and wear technology, ASM International, USA, (1992).

[34] Bhushan B., Introduction to Tribology, John Wiley and Sons, USA, (2002).

[35] Chinn, R.E., Ceramography: Preparation and Analysis of Ceramic Microstructures, ASM International, USA, (2002).

[36] Ragav P. Panakarajupally, R.P., Mirza, F., Rassi, J.E., Morscher, G.N., Abdi, F., Choi, S., Solid particle erosion behavior of melt-infiltrated SiC/SiC ceramic matrix composites (CMCs) in a simulated turbine engine environment. Composites Part B, 216, 108860 (2021).

[37] Bhushan B., Introduction to Tribology, John Wiley and Sons, USA. (2002).

Vol. 16(2) 2021 – ISSN 1331-7210

Engineering Power – *Bulletin of the Croatian Academy of Engineering*

Publisher: Croatian Academy of Engineering (HATZ), 28 Kačić Street, P.O. Box 14, HR-10001 Zagreb, Republic of Croatia

Editor-in-Chief: Prof. Vladimir Andročec, Ph.D., President of the Academy retired Full Professor with tenure, University of Zagreb, Faculty of Civil Engineering

Editor: Prof. Zdravko Terze, Ph.D., Vice-President of the Academy University of Zagreb, Faculty of Mechanical Engineering and Naval Architecture

Guest-Editor: Prof. Lidija Ćurković, Ph.D., University of Zagreb, Faculty of Mechanical Engineering and Naval Architecture

Editorial Board: Prof. Vladimir Andročec, Ph.D., Prof. Zdravko Terze, Ph.D., Prof. Vladimir Mrša, Ph.D.

Editorial Board Address: Croatian Academy of Engineering (HATZ), "Engineering Power" – Bulletin of the Croatian Academy of Engineering, Editorial Board, 28 Kačić Street, P.O. Box 14, HR-10001 Zagreb, Republic of Croatia

E-mail: hatz@hatz.hr

Graphical and Technical Editor: Minerva Graphica, Ltd., Zagreb

Proof-reader: Miroslav Horvatić, MA

Press: Tiskara Zelina, Ltd., Zelina

Circulation: 200